UC Berkeley
UC Berkeley Previously Published Works

Title
Stable Engineered Trimetallic Oxide Scaffold as a Catalyst for Enhanced Solvent-Free Conversion of CO2 into Value-Added Products

Permalink
https://escholarship.org/uc/item/87t2j9xx

Journal
Energy & Fuels, 37(2)

ISSN
0887-0624

Authors
Prasad, Divya
Srinivasappa, Puneethkumar M
Raju, Navya Anna
et al.

Publication Date
2023-01-19

DOI
10.1021/acs.energyfuels.2c03513

Peer reviewed

Stable Engineered Trimetallic Oxide Scaffold as a Catalyst for Enhanced Solvent-Free Conversion of CO_2 into Value-Added Products

Divya Prasad, Puneethkumar M. Srinivasappa, Navya Anna Raju, Akshaya K. Samal, and Arvind H. Jadhav*

Read Online

ACCESS | Metrics & More | Article Recommendations

ABSTRACT: This work demonstrates the development of mesoporous trimetallic oxide scaffolds (TOSs) as heterogeneous catalysts for the solvent-free transformation of CO_2 into various value-added products. The TOS catalyst was prepared using a solution-combustion protocol as a time- and energy-saving method using cobalt, magnesium, and cerium metal nitrate salts as precursors and ethylene glycol as the fuel system and compared with their monometallic counterparts. Characterization suggested strong metal−metal and metal−oxygen interactions in the 3D-interconnected hierarchical porous network, which resulted in substantial alteration in the electronic, structural, and physico-chemical properties. This resulted in an appreciable surface area, acid−base cooperative sites, and a larger pore volume in the catalyst. Thereafter, the CoMgCe-TOS catalyst was first used for the solvent-free cyclization of *o*-phenylenediamines and CO_2 to produce benzimidazoles. In the presence of dimethylamine borane as a reductant, benzimidazoles were obtained in 94% yield at 100 °C under pressurized conditions, along with good recyclability for 12 cycles. It was established that selectivity toward benzimidazole improved upon the incorporation of basic metals (Mg and Ce), with Co aiding in the formation of cooperative Lewis acid−base sites. A plausible mechanism was also predicted, wherein the overall conversion of reactants for the N-formylation step was influenced by the number and strength of basic sites, and the cyclization step for selectively obtaining benzimidazole was affected by the acidic site strength. Besides the production of benzimidazole, the catalyst was also highly active for the synthesis of cyclic carbonates using epoxides and CO_2 under optimized reaction conditions. This work therefore provides a new and greener route for the synthesis of benzimidazoles and organic carbonates, which can be easily adapted for scale-up applications.
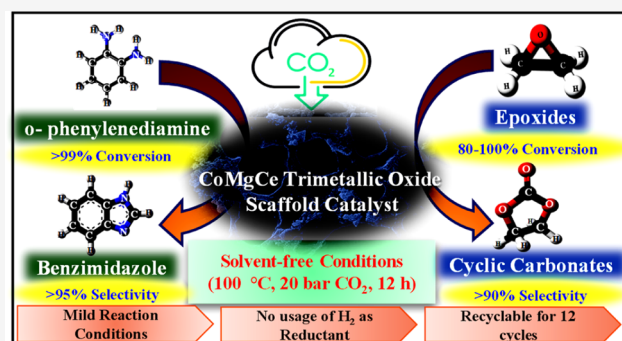
1. INTRODUCTION

Global CO_2 emissions stand as a major impediment to the development of a sustainable society, hence driving the adoption of green chemistry concepts. These emissions are commonly regarded as a major contributor to concerns such as climate change and global warming.[1,2] As a result, the use of CO_2 as a nonflammable, nontoxic, inexpensive, and abundant C1 source for the production of value-added products and commodity chemicals, in order to meet rising human demands and society's long-term growth, has gotten a lot of attention.[3,4] Despite the fact that CO_2 is chemically inert in both thermodynamic and kinetic aspects,[3,5] various efforts have been made to convert CO_2 into a variety of useful products, including cyclic carbonate,[6,7] methane,[8] methanol,[9,10] and N-containing compounds.[9] Particularly, from the standpoint of sustainability factor and green chemistry, the reductive functionalization of amine and CO_2 through the formation of a C−N bond into N-containing heterocycles, such as

benzimidazoles, has recently garnered immense scientific attention.[11] Benzimidazoles are a common skeletal backbone found in physiologically active compounds, natural products,[12] pesticides,[13] and other materials. They are also used for the synthesis of antipsychotic, anthelminthic, anticancer, anti-bacterial, and antihypertensive medications.[14] In addition to medicinal chemistry, benzimidazole derivatives are employed for use in fuel cell electrolytes, optical sensors, supramolecular assemblies, and corrosion inhibitors, to name a few.[14]
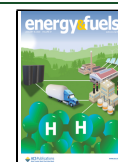
In traditional methods, benzimidazoles are synthesized through reductive cyclization and the formation of C−N bonds using specific amines and a carbon source as reactants.[11] Different molecules, such as N,N-dimethylformamide,[15] dimethoxyethane,[16] formic acid,[17] and methanol,[18] have been used for the production of benzimidazole. Although the above carbon sources can produce a high yield of benzimidazoles, some downsides, such as toxicity and high cost, are unavoidable. As a result, it would be ideal to create a method for using CO_2 as a renewable, affordable, and nontoxic reactant/substrate for the production of benzimidazoles from energy-saving and sustainable standpoints. Also, in general, the reduction reaction of amine and CO_2 requires the employment of a reductant. Hydrogen-containing materials, such as pure hydrogen (H_2) gas,[19] hydroborane,[20] hydrosilane,[21] and their derivatives, have all been employed in the selective manufacture of benzimidazoles, wherein hydrogen is a notoriously inconvenient gas to handle and store. As a result, more emphasis has been paid to the activation of hydroborane as they have high hydrogen storage capacity, use lesser energy, are cost-effective, easier to handle, and less toxic in comparison to hydrosilanes, which are easier to operate and use less energy.[20] Among different hydroboranes, dimethylamine borane (DMAB) is a safer H_2 replacement as it is nonflammable, water-soluble, stable, and has received little attention for such reactions.[20] Therefore, the construction of C−N bonds via the insertion of CO_2 into o-phenylenediamine using DMAB as a reductant to synthesize benzimidazole appears to be a greener strategy. Several metal-based catalysts have been explored for the title reaction in the presence of amine borane, according to previous findings.[20] Even though appreciable results were obtained, these catalytic systems were not cost-effective, produced byproducts, and required harsh reaction conditions, which inhibit their large-scale utility in industries.

The development of metal oxides using solution combustion synthesis methods is considered to be one of the most simple, single-step, and energy-preserving strategies.[22] Usually, metal nitrate precursors are selected because the nitrate groups are reported to be excellent oxidizers and decompose after self-ignition at lower temperatures in the presence of fuels containing carbon and hydrogen, such as ethylene glycol, citric acid, urea, and glycerol.[22] The generation of excess gases in the course of the combustion leads to the development of metal oxides, thereby generating a large number of pores and resulting in a scaffold-like appearance. In contemporary catalytic reactions with CO_2 and amines as reactants, an acid−base bifunctional catalyst along with a suitable reductant is considered pivotal for the synthesis of benzimidazoles.[23] Hence, in this work, acidic and basic metal nitrate precursors of cobalt, magnesium, and cerium were considered oxidizers, and ethylene glycol was chosen as the fuel.

As mentioned above, as part of our ongoing interest in heterogeneous catalytic systems promoted by metal oxide-based catalysts, we present herein the first use of a mesoporous trimetallic oxide scaffold (TOS) prepared using a cost-effective, quick, and energy-saving one-step solution combustion synthesis strategy at lower temperatures when compared to catalysts synthesized by traditional methods. After systematic characterization of the TOSs with its mono-metallic oxide counterparts, they were explored as catalysts for the transformation and cyclization of CO_2 into benzimidazoles under co-catalyst free, solvent-free, and mild reaction conditions.

Additionally, the effect of different reaction variables on the catalytic activity were also explored, following which recyclability studies were performed. A plausible reaction mechanism for the synthesis of benzimidazole using the TOS catalyst was also proposed based on obtained characterization and experimental results. In addition, the TOS acted as a multitasking and versatile catalyst for the synthesis of cyclic carbonates under optimized reaction conditions. To the best of our knowledge, TOSs, as heterogeneous catalysts synthesized using the solution combustion synthesis method, have not been reported for the synthesis of such important compounds. In addition, the high catalytic activity and good recyclability observed for the TOSs obtained using a one-step low-temperature strategy have emphasized the utility of the protocol employed.

2. EXPERIMENTAL SECTION

2.1. Materials. Analytical grade cobalt nitrate hexahydrate ([$Co(NO_3)_2 \cdot 6H_2O$], 99% purity), magnesium nitrate hexahydrate ([$Mg(NO_3)_2 \cdot 6H_2O$], 99% purity), ceric ammonium nitrate ([$(NH_4)_2Ce(NO_3)_6$], 99% purity), and ethylene glycol ([$(CH_2OH)_2$, 99% purity) were obtained from Sigma-Aldrich Pvt. Ltd. and used as received.

For investigating the catalytic reactions, CO_2 (99.999%) was obtained from Balaji Enterprises Pvt. Ltd., India. DMAB (98% purity), o-phenylenediamine (1a: 98% purity), 4-chloro-o-phenyl-enediamine (1b: 97% purity), 4-methyl-o-phenylenediamine (1c: 98% purity), 2-aminothiophenol (1d: 97%), 2-aminophenol (1e: 98%), styrene oxide (2a: 98% purity), propylene oxide (2b: 98% purity), butylene oxide (2c: 98% purity), cyclohexene oxide (2d: 98% purity), epichlorohydrin (2e: 98% purity), potassium carbonate (K_2CO_3, 98% purity), sodium carbonate (Na_2CO_3, 98% purity), cesium carbonate (Cs_2CO_3, 98% purity), calcium carbonate ($CaCO_3$, 98% purity), potassium hydroxide (KOH, 99% purity), tertiary potassium butoxide (^tBuOK, 98% purity), potassium acetate (CH_3CO_2K, 98% purity), and tetrabutylammonium iodide (TBAI) (98% purity) were purchased from Sigma Aldrich Pvt. Ltd., India and used without any modification.

2.2. Synthesis of the CoMgCe-TOS Catalyst. The CoMgCe-TOS catalyst was synthesized using a facile, one-step, energy-conserving solution combustion synthesis strategy. In a typical procedure, 50 wt % of $Co(NO_3)_2 \cdot 6H_2O$, 37.5 wt % of $Mg(NO_3)_2 \cdot 6H_2O$, and 12.5 wt % of $(NH_4)_2Ce(NO_3)_6$ as main oxidizers were blended at room temperature with 1.8 mL of ethylene glycol as fuel in a 25 mL beaker on a magnetic stirrer (450 rpm). After the blended solution attained homogeneity, it was sonicated in an ultrasonic bath for 1 h. Prior to initiating the blending process, an empty petridish was placed in a muffle furnace and heated to 300 °C. The sonicated reaction mixture was evenly poured to this preheated petridish, wherein a spontaneous ignition and self-combustion process took place with the release of large amounts of gases such as CO_2, H_2O, and NO_2. The complete combustion process took approximately 5 min, whereas the actual ignition time was less than 5 s. This self-combustion process led to the formation of scaffold-like, foamy, and porous powder. The resultant powder was collected after cooling down and designated as CoMgCe-TOS or CoMgCe-TOS catalyst. In addition, single metal oxides, namely Co_3O_4, MgO, and CeO_2, with their respective metal nitrate precursors, were prepared using similar methodology for comparison.

2.3. Characterization Techniques. X-ray diffraction (XRD) technique was performed on a Rigaku Ultima IV (Rigaku Corporation, Japan) X-ray diffractometer using Ni-filtered Cu Kα radiation (λ = 1.5406 Å, 30 kV voltage, 15 mA current). The data was recorded at a scan rate of 3° min^{-1} in the 2θ range of 10−80° for single metal oxides and CoMgCe-TOS catalysts to confirm their identification of crystallographic nature, and the crystallite size was calculated using the standard Debye−Scherrer equation. The scaffold-like porous morphology of the final CoMgCe-TOS catalyst was

confirmed using field emission scanning electron microscopy (FE-SEM; JEOL JSM-7100F, Singapore). X-ray photoelectron spectroscopy (XPS) analysis was performed in a PerkinElmer, PHI1257 hemispherical electron energy analyzer at room temperature using a nonmonochromatized Al Kα source with an excitation energy of 1486.7 eV and 4×10^{-10} Torr pressure. The determination of functional groups for single metal oxides and CoMgCe-TOS catalysts was done by performing Fourier transform infrared (FT-IR) spectroscopy of pressed KBr pellets with samples in a PerkinElmer FT-IR instrument in the range of 500−4000 cm^{-1}.

Further, Brunauer−Emmett−Teller (BET) and Barrett−Joyner−Halenda (BJH) methods were used to confirm the textural properties of single metal oxides and CoMgCe-TOS catalysts on BELSORP-MAX (M/s. Microtrac BEL, Japan) in a N$_2$ atmosphere at a temperature of −196 °C. The catalysts were degassed at 100 °C for 4 h under vacuum prior to analysis. The NH$_3$/CO$_2$ temperature-programed desorption (TPD) analysis was performed in order to identify the presence of acidic and basic sites in single metal oxides and CoMgCe-TOS catalysts. An indigenous TPD set-up with a quartz reactor (length: 300 mm, inner diameter: 6 mm) connected to a six-port valve and a thermal conductivity detector (M/s. Mayura Analyticals Pvt. Ltd., India) was loaded with 50 mg of the respective materials and degassed at 300 °C for 1 h under a He atmosphere and thereafter cooled to 100 °C. Subsequently, at 100 °C the materials were saturated with 5% NH$_3$/5% CO$_2$ gas and 95% He for 0.5 h, following which the respective catalysts were again treated in the presence of a He atmosphere for 0.5 h. Finally, peaks for desorbed gases were obtained using TCD with a gradual increase in temperature from 100 to 750 °C at a ramping rate of 10 °C min^{-1} and further retained for another 0.5 h in an isothermal zone. Similarly, H$_2$ temperature-programed reduction (TPR) was performed to test the redox properties of the material in the same apparatus. 50 mg of sample was loaded and pretreated in a He environment at 300 °C for 1 h and subsequently cooled to 100 °C. Further, the materials were passed through 5% H$_2$/95% Ar with a flow rate of 30 mL min^{-1}. Finally, peaks for desorbed H$_2$ gas were obtained using TCD with a gradual increase in temperature from 100 to 750 °C at a ramping rate of 10 °C min^{-1} and further retained for another 0.5 h in the isothermal zone.

2.4. Representative Procedure for Catalytic Synthesis of Benzimidazoles Using CO$_2$ and 1. In an indigenous 100 mL high-pressure reactor equipped with a magnetic stirrer and an automatic temperature controller, 1 mmol of reactant along with 10 wt % of CoMgCe-TOS catalyst, the desired amount of K$_2$CO$_3$ base, and DMAB as a reductant were loaded in the reactor. The reactor was then degassed with CO$_2$ three times to evacuate atmospheric air and induce a homogeneous CO$_2$ environment. Further, the reactor was pressurized to a constant CO$_2$ pressure at the desired temperature for stipulated amount of time. The reactions were carried out at 100 °C for 12 h of reaction time at a maintained rpm of 650−700. After the completion of 12 h, the reactor was cooled down to room temperature naturally, following which it was depressurized in 20 min. The reaction mixture was further diluted in ethyl acetate, and the CoMgCe-TOS catalyst was recovered using a Whatman filter paper through a simple filtration method. After separating the catalyst, the reaction mixture was worked up with brine solution for two consecutive times, wherein the water-soluble DMAB reductant and the K$_2$CO$_3$ base were extracted in the aqueous layer. The crude product containing an organic (ethyl acetate) layer was collected, dried using anhydrous sodium sulfate, and finally concentrated using a rotary evaporator. The concentrated product mixture was purified by aid of column chromatography with commercial silica gel (mesh size 100−200) for which 100% ethyl acetate was used as eluent to isolate benzimidazole as the pure product. The successful synthesis of benzimidazole was confirmed using gas chromatography (GC; Agilent 7820A, HP-5 column equipped with a TCD detector) and GC−mass spectrometry (GC−MS; Shimadzu QP2010SE GCMS), whereas ^{1}H NMR (Bruker 500 MHz) and ^{13}C NMR (Bruker 125 MHz) spectroscopy techniques were performed to confirm the structure of products using CDCl$_3$ as the solvent. The conversion of o-

phenylenediamaine (C_{OPD}) was calculated using the formula $C_{OPD} = (OPD_{in} - OPD_{out}) \times 100/OPD_{in}$, and the selectivity of benzimidazole (S_{BIM}) was calculated using the formula $S_{BIM} = Y_{BIM} \times 100/C_{OPD}$, where OPD_{in} is the amount of OPD at the inlet and OPD_{out} is the amount of OPD in the reaction mass. Y_{BIM} is the corresponding yield of BIM or benzimidazole.

The recovered catalyst was washed with water and ethanol and dried in the oven at 90 °C overnight and reused as catalyst for the next set of reaction. Likewise, the other benzimidazole and N-heterocyclic derivatives were achieved using the same procedure by using the corresponding substituted o-phenylenediamine and respective starting materials and CO$_2$ under the same reaction conditions. The spectroscopic data of all compounds was found to be well in accordance with previously reported literature.

2.4.1. 1H-Benzo[d]imidazole (Table 5, Entry 1). ^{1}H NMR (400 MHz, CDCl$_3$): δ 9.05 (s, 1H), 8.10 (s, 1H), 7.64 (d, J = 4.0 Hz, 2H), 7.28−7.25 (m, 2H); ^{13}C NMR (125 MHz, CDCl$_3$): δ 140.7, 137.1, 123.0, 115.4; IR (cm^{-1}): 3459 (N−H str.), 2993 (C−H str.), 1741 (C=O str. of ethylacetate), 1517 (N−H bend.), 1377 (C−N str.), 1231 (C−O str. of ethylacetate); GC−MS: C$_7$H$_6$N$_2$ [M]$^+$, 118.14; found, 118.1.

2.4.2. 5-Chloro-1H-benzo[d]imidazole (Table 5, Entry 2). ^{1}H NMR (400 MHz, CDCl$_3$): δ 8.09 (s, 1H), 7.65 (d, J = 1.2 Hz, 1H), 7.58 (d, J = 8.4 Hz, 1H), 7.38 (s, 1H); IR (cm^{-1}): 3462 (N−H str.), 2974 (C−H str.), 1735 (C=O str. of ethylacetate), 1410 (N−H bend.), 1369 (C−N str.), 1229 (C−O str. of ethylacetate), 747 (C−Cl str.); GC−MS: C$_7$H$_5$ClN$_2$ [M]$^+$, 152.58; found, 152.1.

2.4.3. 5-Methyl-1H-benzo[d]imidazole (Table 5, Entry 3). ^{1}H NMR (400 MHz, CDCl$_3$): δ 8.02 (s, 1H), 7.56 (d, J = 8.0 Hz, 1H), 7.44 (s, 1H), 7.12 (d, J = 8.0 Hz, 1H), 2.48 (s, 3H); IR (cm^{-1}): 3467 (N−H str.), 2986 (C−H str.), 1729 (C=O str. of ethylacetate), 1441 (N−H bend.), 1374 (C−N str.), 1247 (C−O str. of ethylacetate); GC−MS: C$_8$H$_8$N$_2$ [M]$^+$: 132.16; found: 132.0.

2.4.4. Benzo[d]oxazole (Table 5, Entry 4). ^{1}H NMR (400 MHz, CDCl$_3$): δ 8.28 (s, 1H), 7.20−7.25 (m, 2H), 7.03 (t, J = 7.2 Hz, 2H); IR (cm^{-1}): 3101 (C−H str.), 1450 (C=C str.), 1236 (C−N str.), 1056 (C−O str.); GC−MS: C$_7$H$_5$NO [M]$^+$: 119.12; found: 118.1.

2.4.5. Benzo[d]thiazole (Table 5, Entry 5). ^{1}H NMR (400 MHz, CDCl$_3$): δ 9.00 (s, 1H), 8.15 (d, J = 8.0 Hz, 1H), 7.98 (d, J = 7.6 Hz, 1H), 7.55−7.44 (m, 2H); IR (cm^{-1}): 3052 (C−H str.), 1422 (C=C str.), 1282 (C−N str.), 1050 (C−S str.); GC−MS: C$_7$H$_5$NS [M]$^+$, 135.19; found, 135.0.

2.5. Representative Procedure for Catalytic Synthesis of Cyclic Carbonates Using CO$_2$ and Epoxides. All cycloaddition reactions for the conversion of epoxides and CO$_2$ were performed in the same indigenous high-pressure reactor equipped with a magnetic stirrer and automatic temperature controller. The reactor was charged with epoxide (8.3 mmol), catalyst (10 wt %, 10 mg), and TBAI (0.2 mmol) at room temperature. Further, the reactor was purged with CO$_2$ three times to attain homogeneity, following which the CO$_2$ pressure was adjusted to 20 bar. The rpm rate was maintained at 650−700, and the cycloaddition reaction was performed at 100 °C for 12 h. After the completion of the reaction, the reactor was cooled to room temperature and slowly depressurized to atmospheric pressure. The brown-colored reaction mixture was then extracted using ethyl acetate, and the catalyst was separated using a Whatman filter paper and analyzed using GC and GCMS techniques.

3. RESULTS AND DISCUSSION

The synthesis of metal oxides using solution combustion synthesis has been reported to be a highly exothermic method which is accompanied by the release of large amounts of gases such as CO$_2$, NO$_2$, and H$_2$O. The fuel used during the synthesis plays a paramount role to initiate the combustion reaction with the oxidants. In addition, the fuel acts as a reducer, a microstructural template, as well as a complexing agent. Herein, a three-dimensional CoMgCe-TOS was synthesized using a one-step solution combustion synthesis
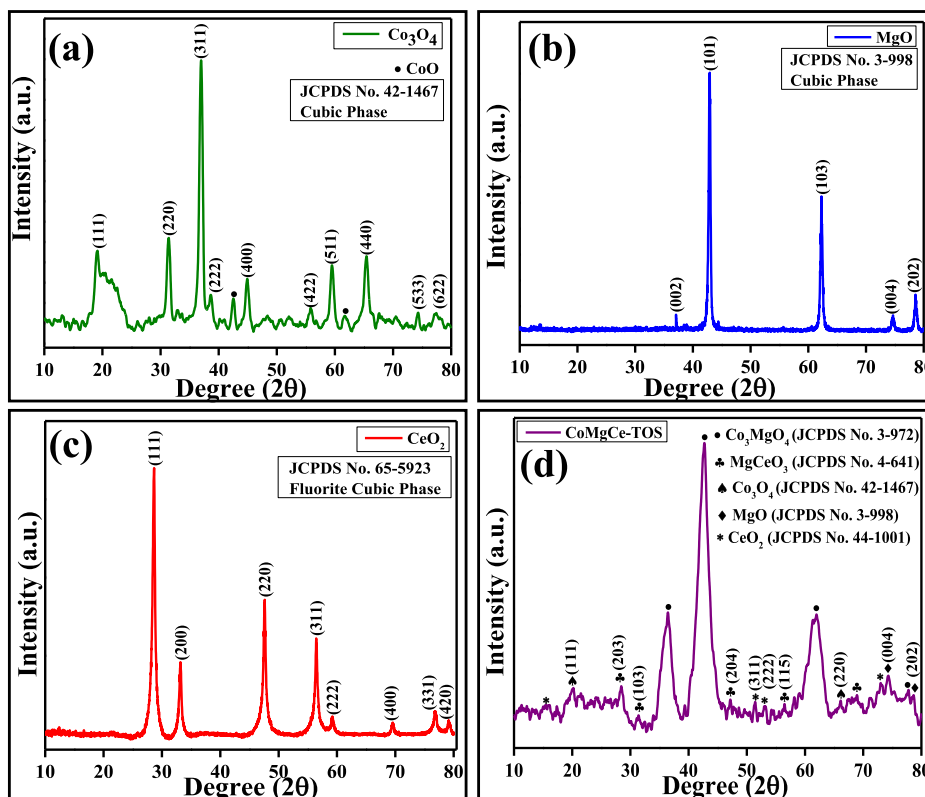
Figure 1. XRD diffractograms of single metal oxides (a) Co_3O_4, (b) MgO, and (c) CeO_2 and of (d) CoMgCe-TOS catalyst.
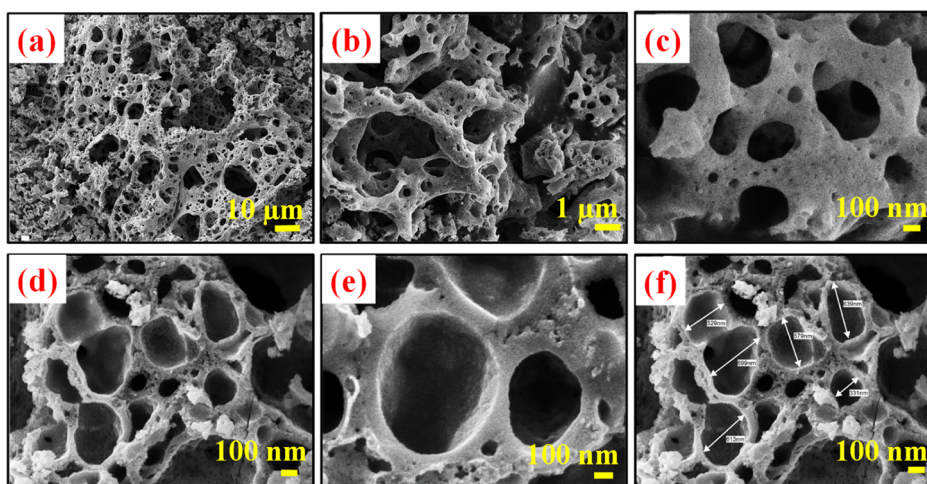

Figure 2. (a−f) FE-SEM analysis of the CoMgCe-TOS catalyst.

protocol, wherein ethylene glycol was used as a fuel for the combustion, which subsequently got oxidized by the nitrate ions. An advantage of porous scaffold-like morphology obtained by the solution combustion synthesis method is the enormous content of the pore interconnectivity, which is controlled by the oxidizer and fuel ratios. The porous catalyst obtained was further used in this study for the cyclization of CO_2 into two value-added products, namely benzimidazoles and cyclic carbonates. Prior to this, the scaffold was characterized using various analytical and spectroscopic techniques to gather information about its physicochemical and structural characteristics. Additionally, using the same synthetic protocol, single metal oxides, using the individual nitrate precursors of cobalt, magnesium, and cerium metals in

ethylene glycol were prepared for highlighting a rational comparison between the single metal oxides and the CoMgCe-TOS catalyst.

3.1. XRD Analysis. XRD patterns were recorded in the 2θ range of 10−80° for examining the crystalline phases of the synthesized materials. Figure 1 illustrates the typical XRD diffractograms of the synthesized CoMgCe-TOS catalyst and compared with the single metal oxides. According to the XRD diffractograms, all three single metal oxides displayed strong and sharp crystalline features of pure metal oxides, namely Co_3O_4, MgO, and CeO_2, with no other unidentified peaks.[24−26] As can be seen in Figure 1a, the peaks belonging to the cubic phase of Co_3O_4 (JCPDS no. 42-1467) were positioned at 19.1°(111), 31.4°(220), 36.9°(311), 38.7°(222),
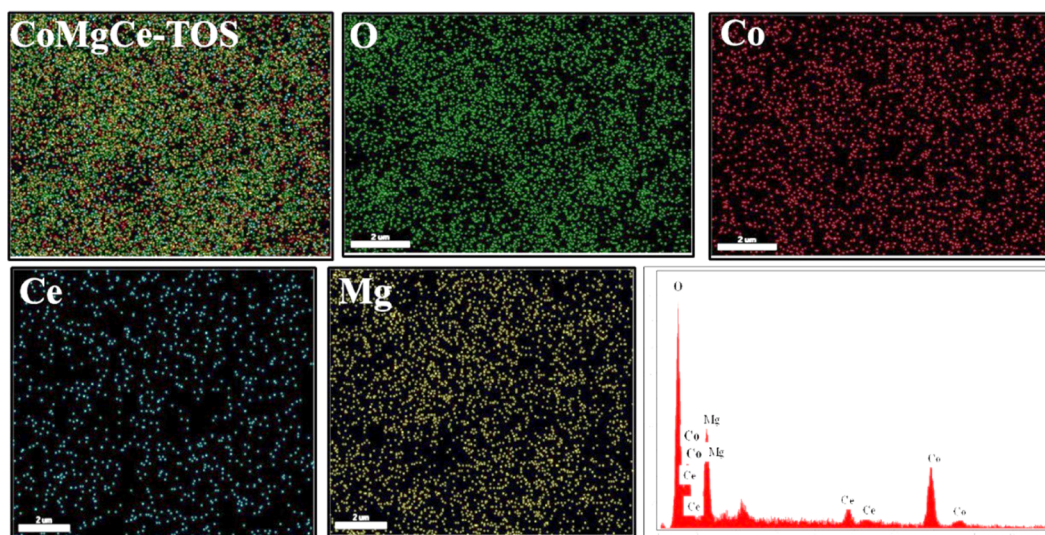
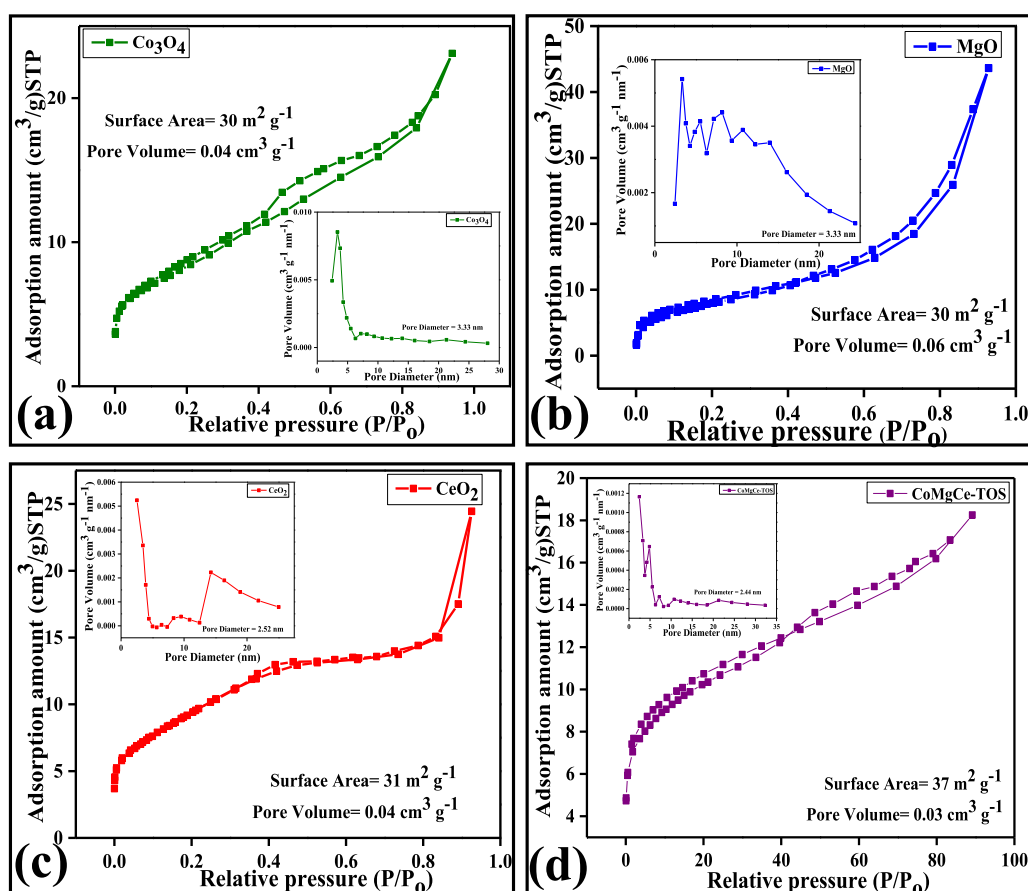**Figure 3.** EDAX and elemental mapping analysis of the CoMgCe-TOS catalyst.

Figure 4. N_2-adsorption−desorption analysis and pore size distribution (inset) of single metal oxides (a) Co_3O_4, (b) MgO, and (c) CeO_2 and of (d) CoMgCe-TOS catalyst.

44.9°(400), 55.6°(422), 59.2°(511), 65.2°(440), 74.3°(533), and 77.6°(022). No additional peaks were observed except for minor contents of the CoO phase in the Co_3O_4 diffractogram.[24] The diffraction peaks in Figure 1b, at 36.8, 42.9, 62.2, 74.7, and 78.3° can be indexed to (002), (101), (103), (004), and (202) planes, respectively, corresponding to the cubic phase of pure MgO (JCPDS no. 3-998).[25] Furthermore, from Figure 1c, it is evident that the diffractogram of CeO_2 indexed

at 28.4°(111), 33.1°(200), 47.5°(220), 56.3°(311), 59.1°(222), 69.5°(400), 76.8°(331), and 79.1°(420) crystal planes corresponds to the fluorite cubic phase (JCPDS no. 65-5923).[26] The crystallite size of Co_3O_4, MgO, and CeO_2 were calculated using the Debye−Scherrer equation and found to be 4.38, 8.94, and 18.12 nm, respectively.

Finally, the CoMgCe-TOS catalyst primarily consisted of Co_3MgO_4 (JCPDS no. 3-972) and $MgCeO_3$ (JCPDS no. 4-
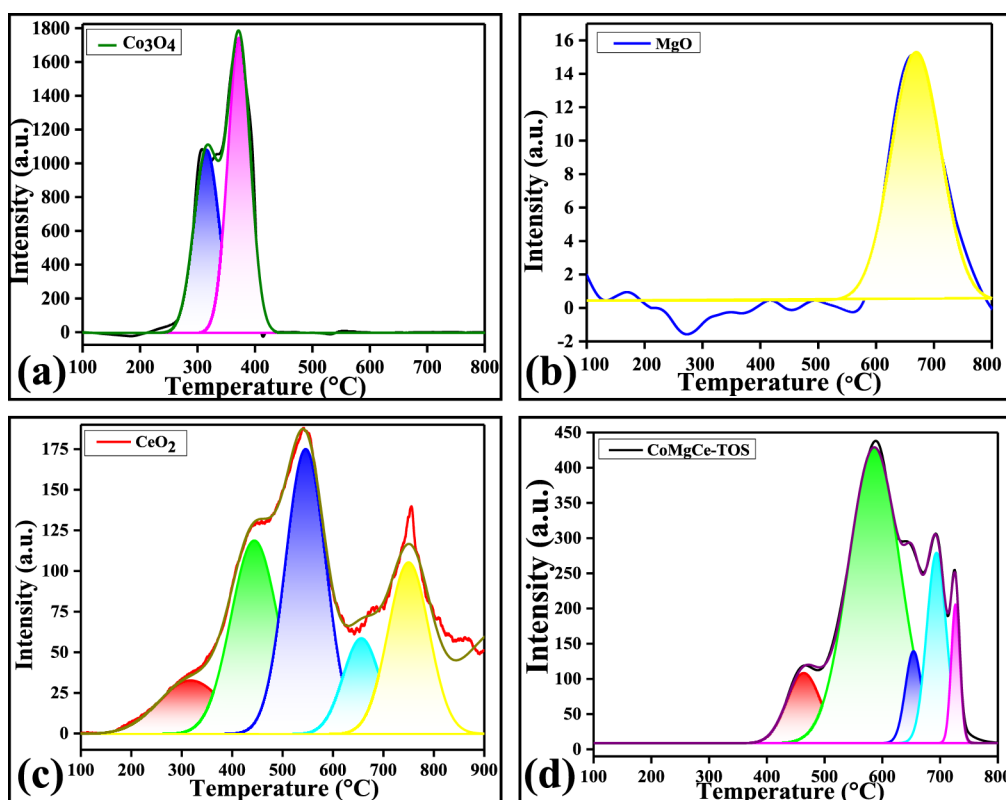
Figure 5. H$_2$-TPR analysis of (a) Co$_3$O$_4$, (b) MgO, (c) CeO$_2$, and (d) CoMgCe-TOS catalyst.

641) cubic phases along with minor quantities of MgO centered at 74.3 and 78.6° and the Co$_3$O$_4$ phase at 20.2 and 66.1°.[27] Further, the minor reflections at 28.1, 47, and 57.2° can be attributed to the presence of the CeO$_2$ phase.[26] As reported by Al-Doghachi et al., the presence of CeO$_2$ in the oxide framework hinders the agglomeration of MgO and Co$_3$O$_4$ leading to a decrease in the crystallite size.[28] This literature was well supported, wherein the crystallite size of the CoMgCe-TOS catalyst was calculated to be 4.06 nm. An overall interpretation suggests that all the single metal oxides and the CoMgCe-TOS catalyst were crystalline in nature, and the crystallinity decreased in the following order: CeO$_2$ > MgO > Co$_3$O$_4$ > CoMgCe-TOS.

3.2. FE-SEM Analysis. The structural architecture of CoMgCe-TOS was characterized using FE-SEM analysis, and the obtained images are displayed in Figure 2. The low-resolution FE-SEM images revealed the presence of highly ordered three-dimensional porous architecture with a large number of homogeneously distributed pores contained in the scaffold network (Figure 2a,b). Interestingly, it can also be observed that the larger pores in the scaffold network were well-interconnected with smaller pores, as evident in Figure 2c,d.[29] The formation of these abundant and dense pores was uniform throughout the surface of the scaffold network. Notably, the generation of these large number of pores was primarily governed by the evolution of nitrate ions from the metal precursors during the self-combustion process.[30,31] A closer view of the scaffold network by arbitrarily sectioning one area provided more insight with regard to the presence of voids and the well-developed porosity of the scaffold (Figure 2e).[30] Moreover, as can be seen in Figure 2f, the size of the pores in CoMgCe-TOS was observed to be in the range of 300−700 nm. It is, hence, evident that apparent presence of large

number of interconnected pores in the scaffold network provided hierarchical porous architecture for CoMgCe-TOS. These interconnected pores might provide space for accessing the catalytically active centers to activate the reactants and facilitate improved reaction kinetics during the catalytic reactions. Moreover, as displayed in Figure 3, energy dispersive X-ray analysis (EDX) and elemental mapping analysis confirmed the stoichiometry and uniform distribution of elements, namely Co, Mg, Ce, and O, in the CoMgCe-TOS catalyst.

3.3. BET and BJH Analyses. N$_2$ adsorption and desorption analysis was performed at liquid N$_2$ temperature (−196 °C) for single metal oxides (Co$_3$O$_4$, MgO, and CeO$_2$) and CoMgCe-TOS in order to determine the surface area and the pore size distribution. The N$_2$-adsorption−desorption isotherms along with the corresponding pore size distribution plots are represented in Figure 4. All the samples showed type-IV isotherms, which is the characteristic feature of mesoporous materials.[32] The single metal oxides namely Co$_3$O$_4$, MgO, and CeO$_2$ exhibited 30, 30, and 31 m^2 g^{-1} of surface area, respectively. Additionally, corresponding pore volumes of 0.04, 0.06, and 0.04 cm^3 g^{-1} were obtained. Similarly, the CoMgCe-TOS catalyst showcased a slightly higher surface area corresponding to 37 m^2 g^{-1} along with a pore volume of 0.03 cm^3 g^{-1}. The increase in surface area of the CoMgCe-TOS catalyst is indicative of the highly porous nature of the TOSs and the uniform distribution of the metal oxides in the CoMgCe-TOS catalyst, as also confirmed from the EDX and SEM analysis.[6] Additionally, upon the formation of scaffolds, the structural properties were influenced by the addition of CeO$_2$, which in turn resulted in the high surface area.[6] Moreover, all the samples showed the H3-hysteresis loop, where P/P^0 had a value greater than 0.4. The presence of H3-
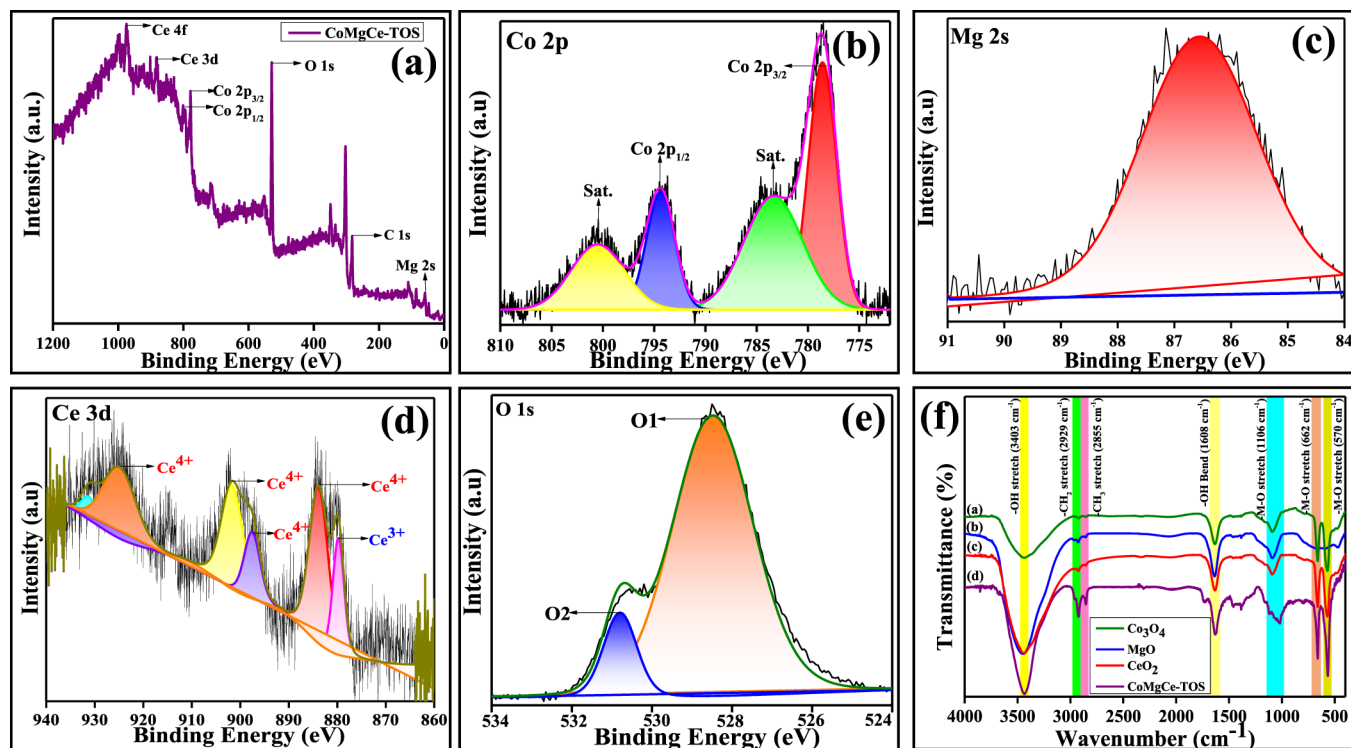
Figure 6. XPS analysis of the CoMgCe-TOS catalyst: (a) XPS full-scan spectrum, (b) Co 2p, (c) Mg 2s, (d) Ce 3d, and (e) O 1s binding energy spectrum. (f) FT-IR spectrum of Co_3O_4, MgO, CeO_2, and CoMgCe-TOS catalyst.

hysteresis loop suggested the presence of a slit-shaped mesoporous structure.[6] Similarly, the presence of mesoporous structure in Co_3O_4, MgO, CeO_2, and CoMgCe-TOS catalysts was also confirmed from the pore size distribution analysis, as calculated by the BJH method, which also supports the existence of the type IV isotherm. The respective pore diameters obtained for Co_3O_4, MgO, CeO_2, and CoMgCe-TOS catalysts were found to be 3.33, 3.33, 2.52, and 2.44 nm. On the basis of the pore volume and pore diameter values obtained for the CoMgCe-TOS catalyst, it can be said that the increase in its surface area could be related to the increased number of smaller, interconnected pores in the 3D scaffold network. The surface of the catalyst can possibly allow proper contact with the reactants and CO_2 and improve catalytic performance.

3.4. H$_2$-TPR Analysis. H_2-TPR studies were performed in an effort to evaluate the redox properties of the single metal oxides and the CoMgCe-TOS catalyst.[33] The obtained profiles are displayed in Figure 5. As displayed in Figure 5a, single metal oxides, namely Co_3O_4, displayed a shoulder peak at 305 °C with a major distinguishable peak centered at 370 °C.[34] The two peaks obtained upon deconvolution can be attributed to the reduction of Co_3O_4 to CoO and the reduction of CoO to metallic Co.[34] This observation is in line with previous literature reports, which confirm the existence of two peaks for pure Co_3O_4.[34] Further, it is well-reported that reduction of MgO takes place at very high temperatures.[35] Therefore, the appearance of a broad reduction peak centered at around 700 °C was related to the reduction of MgO (Figure 5b).[35] On the other hand, for CeO_2 the H_2-TPR profile displayed two well-defined peaks along with three shoulder peaks in the range of 200 and 800 °C (Figure 5a).[36] Upon deconvolution, a small shoulder peak at around 300 °C corresponds to the reduction of surface oxygen species.[37] The two deconvoluted peaks in the

range of 445−540 °C were attributed to the reduction of Ce^{4+}, whereas the broad peak at 750 °C was related to the reduction of bulk CeO_2.[38] Similar observations were reported by Laguna and co-workers.[38]

In the H_2-TPR profile of the CoMgCe-TOS catalyst, as shown in Figure 5d, the apparent reduction of oxides of cobalt, magnesium, and cerium was observed. A general observation suggested that the combination of three metals shifted the T_{max} of the reduction peaks toward higher temperatures.[39] This can be related to the fact that the presence of CeO_2 and MgO makes the overall reduction of the trimetallic CoMgCe oxide difficult.[34] Further, on deconvolution of the same, five peaks were obtained. The first reduction peak at a lower temperature in the range of 460 °C can likely be related to the reduction of highly dispersed Co_3O_4 and surface oxygen species.[40] The second deconvoluted peak at 585 °C along with a shoulder peak at 655 °C could be referred to the reduction of bulk Co_3O_4 and partial reduction of surface ceria species.[41] This observation suggested that more amount of Co^{3+} and Ce^{4+} existed in the CoMgCe-TOS catalyst and was consistent with the XPS results.[39] The two peaks centered at higher temperatures of 695 and 730 °C were due to the reduction of bulk CeO_2 and MgO, respectively.[39] This observation is in line with XRD results, wherein minor peaks of segregated Ce and Mg oxides were evidenced. Based on the H_2-TPR results, it can be concluded that the trimetallic CoMgCe-TOS catalyst showed a higher H_2 consumption value and increased reducibility due to intimate interaction between the respective metals, uniform dispersion, and low crystallite size, as confirmed using XRD analysis. This resulted in improved redox properties when compared to the single metal oxides due to transfer of electrons in the trimetallic system.[39] Hence, it can be assumed that the enhanced reducibility can allow enhanced surface mobility of the oxygen (O_2^-) species,
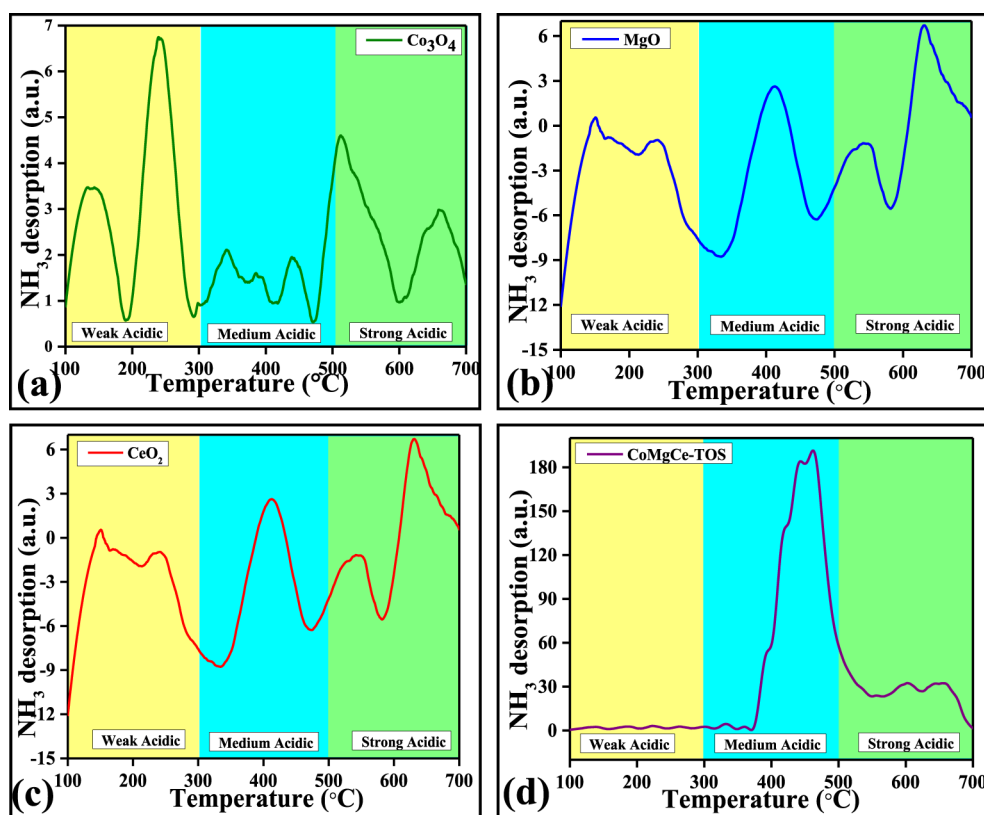
Figure 7. NH$_3$-TPD analysis of (a) Co$_3$O$_4$, (b) MgO, (c) CeO$_2$, and (d) CoMgCe-TOS catalyst.

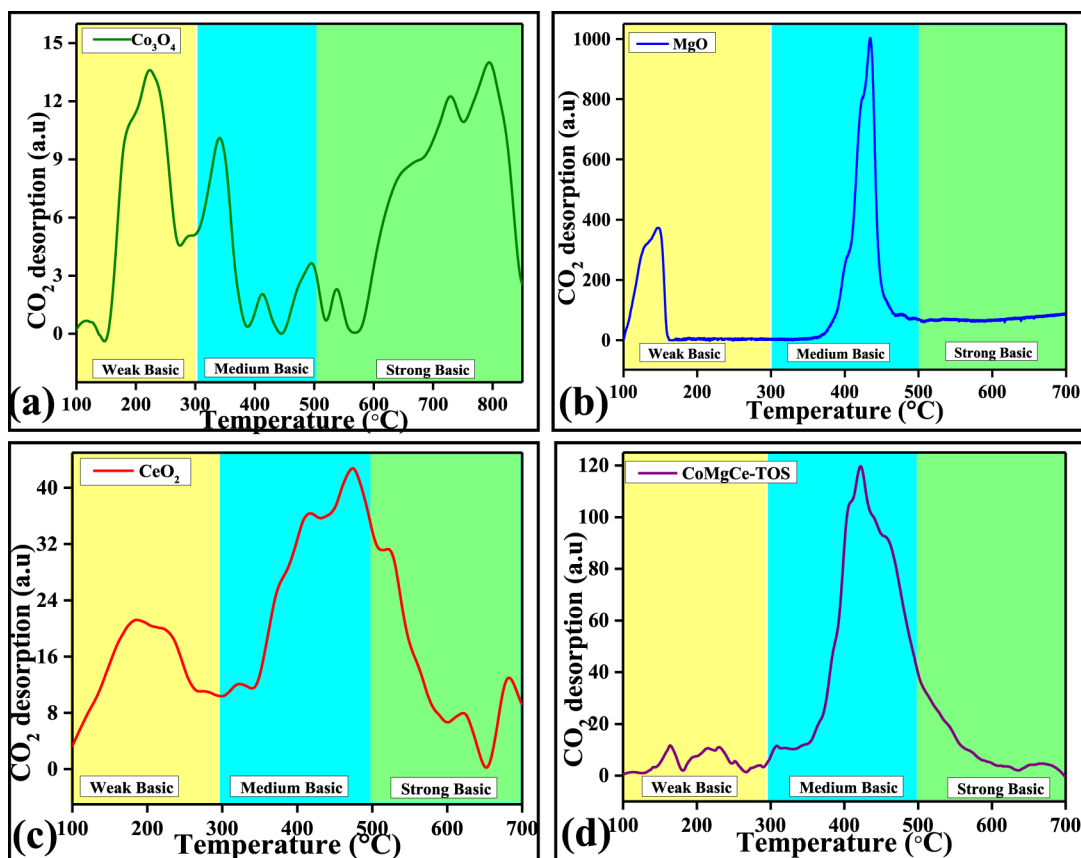thereby enabling better performance during the catalytic CO$_2$ reaction.[39]

3.5. XPS Analysis. A detailed XPS study was performed to study the comprehensive element compositions, the nature of metals, namely cobalt, magnesium, and cerium, and the valence states of oxygen present on the surface of the CoMgCe-TOS catalyst. Figure 6a exhibits the complete survey scan spectra, which illustrates the principal existence of Co 2p, Mg 2s, Ce 3d, and O 1s as core-level peaks. This observation provided excellent support for the successful preparation of the CoMgCe-TOS catalyst using the solution combustion synthesis method. The main peaks along with their corresponding satellite peaks can be clearly identified in the spectra, as displayed in Figure 6b−e. All peaks are in good agreement with those reported in previous literature.[42,43] The valence state of the cobalt ions in the CoMgCe-TOS catalyst was surveyed from the resolved Co 2p spectra using Gaussian peak fitting. It can be clearly seen that the Co 2p peak split into two components, viz. Co 2p$_{3/2}$ and Co 2p$_{1/2}$ along with two shake-up satellite (indicated by "sat.") peaks. The high-resolution Co 2p spectrum displayed BE values of 778.4 and 794.6 eV, assigned to Co 2p$_{3/2}$ and Co 2p$_{1/2}$, respectively. The corresponding satellite peaks for Co 2p$_{3/2}$ and Co 2p$_{1/2}$ levels were also observed at 783.3 eV and 800.9 eV, respectively (Figure 6b). This splitting occurred due to the spin−orbital coupling interactions between the 2p core level and unpaired 3d electrons.[44] This observation confirmed the presence of a specifically mixed oxidation state of Co^{2+} and Co^{3+} in the CoMgCe-TOS catalyst.[44] Typically, the CoMgCe-TOS catalyst showed a higher BE for Co 2p$_{3/2}$ when compared to the BE of pure Co$_3$O$_4$, which accounts for the possibility of electron transfer and synergistic metal−metal interaction of

Co^{2+} with the other metals.[43] Furthermore, as illustrated in Figure 6c, the Gaussian peak-fitted core level Mg 2s spectra exhibited a single peak at BE of 86.5 eV, which is in close agreement with previous literature reports.[42] This peak could be related to the interaction of Mg species with Co because this BE value appears at a lower BE value than that of pure MgO (88.1 eV).[42] Another deconvoluted peak appearing at 88.1 eV can be attributed to the weak interaction of Mg species with Ce species.[45] These observations suggest that Mg interacted with both Co and Ce species, which is well in accordance with XRD analysis.

Furthermore, the XPS spectra of the core-level binding energies of Ce 3d are represented in Figure 6d. The Ce 3d spectra could be deconvoluted into six peaks in the BE range of 860−930 eV.[46] The peaks corresponding to BE values of 883.4, 898.2, and 900.7 eV could be well-fitted to the presence of Ce^{4+} species, whereas Ce^{3+} could be fitted at 880.6 eV.[46] More interestingly, the peaks obtained in the region of 920−930 eV strongly suggested the strong presence of Ce^{4+} species and are usually assigned to the 4f^0 orbital.[47,48] Moreover, the shift in the peak position (916 eV for pure CeO$_2$) to a higher BE value can be attributed to the interaction of Ce with other metallic species.[49] Thus, it can be said that the Ce(3d) spectra of the CoMgCe-TOS catalyst consisted of both Ce^{3+} and Ce^{4+} valence states but predominantly consisted of Ce^{4+} species.[46,49] This observation further supports the XRD results, where the presence of MgCeO$_3$ phase consists of Ce^{4+} species. It is of great importance to realize the nature of oxygen species present in mixed metal oxides.[50] Therefore, the O 1s core level spectra was deconvoluted, as shown in Figure 6e. It can be evidently observed that the BE of O 1s showed two contributory deconvolution peaks. The peak at 529.4 eV can

Table 1. Textural Properties of Single Metal Oxides and CoMgCe-TOS Catalysts

sr. no	catalyst	BET surface area (m² g⁻¹)	pore diameter (nm)	pore volume (cm³ g⁻¹)	crystallite size (nm)	acidic sites (mmol g⁻¹)	basic sites (mmol g⁻¹)
1	Co_3O_4	30	3.33	0.04	4.38	5.58	0.33
2	MgO	30	3.33	0.06	8.94	1.52	8.17
3	CeO_2	31	2.52	0.04	18.12	2.74	7.60
4	CoMgCe-TOS	37	2.44	0.03	4.06	4.06	3.38

Figure 8. CO_2-TPD analysis of single metal oxides (a) Co_3O_4, (b) MgO, and (c) CeO_2 and of (d) CoMgCe-TOS catalyst.

be attributed to the typical presence of metal−oxygen bonds or lattice O^{2-} species.[44] The peak present at 531.6 eV can be ascribed to uncoordinated lattice oxygen, surface hydroxyl, and chemisorbed oxygen species. The XPS results can be well-matched with the H_2-TPR results, wherein the reduction temperature increased when compared to the single metal oxides due to strong and synergistic metal−metal and metal−oxygen interactions in the CoMgCe-TOS catalyst.[43]

3.6. FT-IR Analysis. FT-IR spectroscopy was employed for the identification of vibrational modes and bond formations of the CoMgCe-TOS catalyst. The FT-IR spectra of the synthesized single metal oxides prepared using the solution combustion synthesis method were also performed for comparison. The obtained spectra are presented in Figure 6f. Interestingly, all four materials showed typical characteristic peaks of metal oxides.[22,49] Two additional bands were observed in the range of 3000−3700 cm⁻¹ centered at 3403 cm⁻¹ along with another band at 1626 cm⁻¹ attributed to the −OH stretching and bending modes of adsorbed water, respectively.[51] The minor absorption bands at 2929 and 2855 cm⁻¹ can be assigned to the stretching vibration of the C−H bonds, attributed to the small but negligible amount of ethylene glycol.[22] Notably, the peaks observed in the range of

500−1100 cm⁻¹ can be attributed to typical metal oxide bonds.[22] Especially, the peaks situated at 570 and 662 cm⁻¹ were associated with stretching vibrational modes of M−O (M = Co, Mg, and Ce) bonds. Based on the abovementioned results, it was confirmed that single metal oxides and the CoMgCe-TOS catalyst were effectively formed and well matched with the XRD and XPS results.

3.7. NH₃-TPD Analysis. The quantitative estimation along with the strength of the acidic and basic sites were determined using NH_3 and CO_2-TPD studies, respectively.[6,52] Typically, the temperature range of desorption peaks designate the strength of the acidic and basic sites.[52] The strength of these sites is primarily classified into three types namely weak sites (100−300 °C), moderate sites (300−500 °C), and strong sites (>500 °C).[53] Furthermore, desorption peak area reflects upon the amount of desorbed NH_3 or CO_2 gas, which corresponds to the total number of acidic or basic sites.[53] The related surface acidity of the single metal oxides and CoMgCe-TOS catalyst were measured using NH_3 as a probe molecule.[54] The acquired NH_3-TPD desorption profiles are represented in Figure 7.

As shown in Figure 7a, single metal oxide, namely Co_3O_4, exhibited numerous desorption peaks in all three regions.[55]

Table 2. Optimization of Initial Reaction parameters[a]
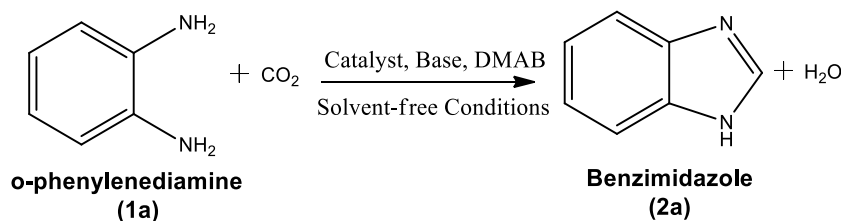
sr. no.	catalyst (mg)	conversion[e] (%)	selectivity[e] (%)	yield[e] (%)
1	no DMAB, no catalyst, no base	0	0	0
2	no DMAB[b]	27	11	3
3	no catalyst[c]	19	32	6
4	no base[d]	99	27	26
5	pure CeO₂	99	79	78
6	pure MgO	99	69	68
7	pure Co₃O₄	99	56	55
8	MgCoCe	99	87	86
9	**CoMgCe**	**99**	**95**	**94**
10	CeCoMg	99	90	89

[a]Reaction conditions: 1 mmol OPD, 10 wt % CoMgCe catalyst, 0.5 mmol K_2CO_3 base, and 3 mmol DMAB, 20 bar CO_2 pressure, 12 h. [b]Reaction conditions: 10 wt % CoMgCe catalyst and 0.5 mmol K_2CO_3 base. [c]Reaction conditions: 0.5 mmol K_2CO_3 base and 3 mmol DMAB. [d]Reaction conditions: 10 wt % CoMgCe catalyst and 3 mmol DMAB. [e]Conversion, yield, and selectivity of cyclic carbonate were determined using GC and GC−MS analyses.

The most intense desorption peaks were centered in the weakly and strongly acidic regions (140, 240, 500, and 660 °C) along with minor peaks in the moderately acidic regions, indicating the presence of a wide range of surface acidic sites.[55] In addition, MgO and CeO₂ also showed NH_3 desorption peaks in all three weak, moderate, and strong regions (Figure 7b,c).[56] However, the intensities of these peaks were lower, as a result of their more basic nature.[56] According to previous literature reports, the NH_4^+ ions coordinated at the Bronsted acidic sites are usually less thermally stable than the NH_3 coordinated at the Lewis acidic sites.[56] Hence, it can be conjectured that the presence of desorption peaks in the lower temperature regions (<300 °C) in Figure 7a−c were due to loosely bound NH_4^+ molecules on the Bronsted acidic sites, whereas the presence of desorption peaks at higher temperature regions corresponded to the presence of Lewis acidic sites.[57]

Interestingly, the CoMgCe-TOS catalyst prepared using a combination of these three metals displayed a major desorption peak spread in the temperature range of 370−550 °C, with maximum intensity between 440 and 465 °C (Figure 7d). This desorption temperature range suggested that the surface of the CoMgCe-TOS catalyst predominantly consisted of a greater number of Lewis acidic sites, possibly caused by the strong metal−metal interaction.[45] This further implied that the Co, Mg, and Ce within the CoMgCe-TOS catalyst played a synergistic role toward the formation of Lewis acidic sites.[45,58] Additionally, a small but reasonable amount of strongly acidic sites were identified at temperatures >550 °C, with two broad peaks centered at 600 and 650 °C.[57] According to Dai and co-workers, the appearance of such broad peaks at higher temperatures can be attributed to the stronger interaction of the NH_3 molecule and enhancement toward Lewis acidic sites.[59] Furthermore, the reduction in the number of strongly acidic sites could possibly be caused by the basic nature of MgO and CeO₂ which, owing to their strong metal oxygen bonds, could suppress the acidity in the CoMgCe-TOS

catalyst. Finally, the amount of desorbed NH_3 was quantified by deconvoluting the area under the desorption curve and tabulated in Table 1. Based on the results obtained, it can be said that the CoMgCe-TOS catalyst possessed an appreciable number of Lewis acidic sites, which could be ascribed to the strong metal−metal/oxide interaction and uniform distribution of the metals themselves.

3.8. CO_2-TPD Analysis. According to Jadhav et al., the adsorption of CO_2 on the active basic sites followed by its subsequent activation plays a pivotal role in CO_2 transformation reactions.[6] In this regard, CO_2-TPD analysis provided insights on the amount of surface basic sites and basic strength of the single metal oxides and the CoMgCe-TOS catalyst. The obtained CO_2-TPD profiles are displayed in Figure 8. As represented in Figure 8a−c, the desorption profiles of single metal oxides namely Co₃O₄, MgO, and CeO₂ presented peaks of lesser intensity at temperatures <200 °C, corresponding to the weak basic sites.[52] Furthermore, the presence of peaks in the range of 300−500 °C in MgO and CeO₂ belonged to dominant basic sites of moderate strength.[52,60] At temperatures >500 °C, especially in case of Co₃O₄ and CeO₂, the presence of less-intense peaks originated from the presence of small amount of strong basic sites.[61] The surface basic density of MgO was the highest among all the studied single metal oxides, followed by CeO₂ and Co₃O₄.[62,63]

Finally, the CO_2-TPD profile of the CoMgCe-TOS catalyst displays peaks in all three temperature regions, mainly depicting three types of active basic sites.[45] As shown in Figure 8d, weak desorption peaks at temperatures <300 °C suggest the presence of small amount of loosely bound and surface adsorbed oxygen groups belonging to weakly basic sites.[6] A major volcano-shaped desorption peak was obtained in the range of 300−570 °C, suggesting the presence of metal−oxygen (M−O) bonds and/or lattice oxygen species.[45,64] Also, as reported by Xu et al., moderate basic sites can be developed in mixed metal oxides containing basic metals due to the adsorption of CO_2 on the basic metal−oxygen sites.[64] Lastly, a
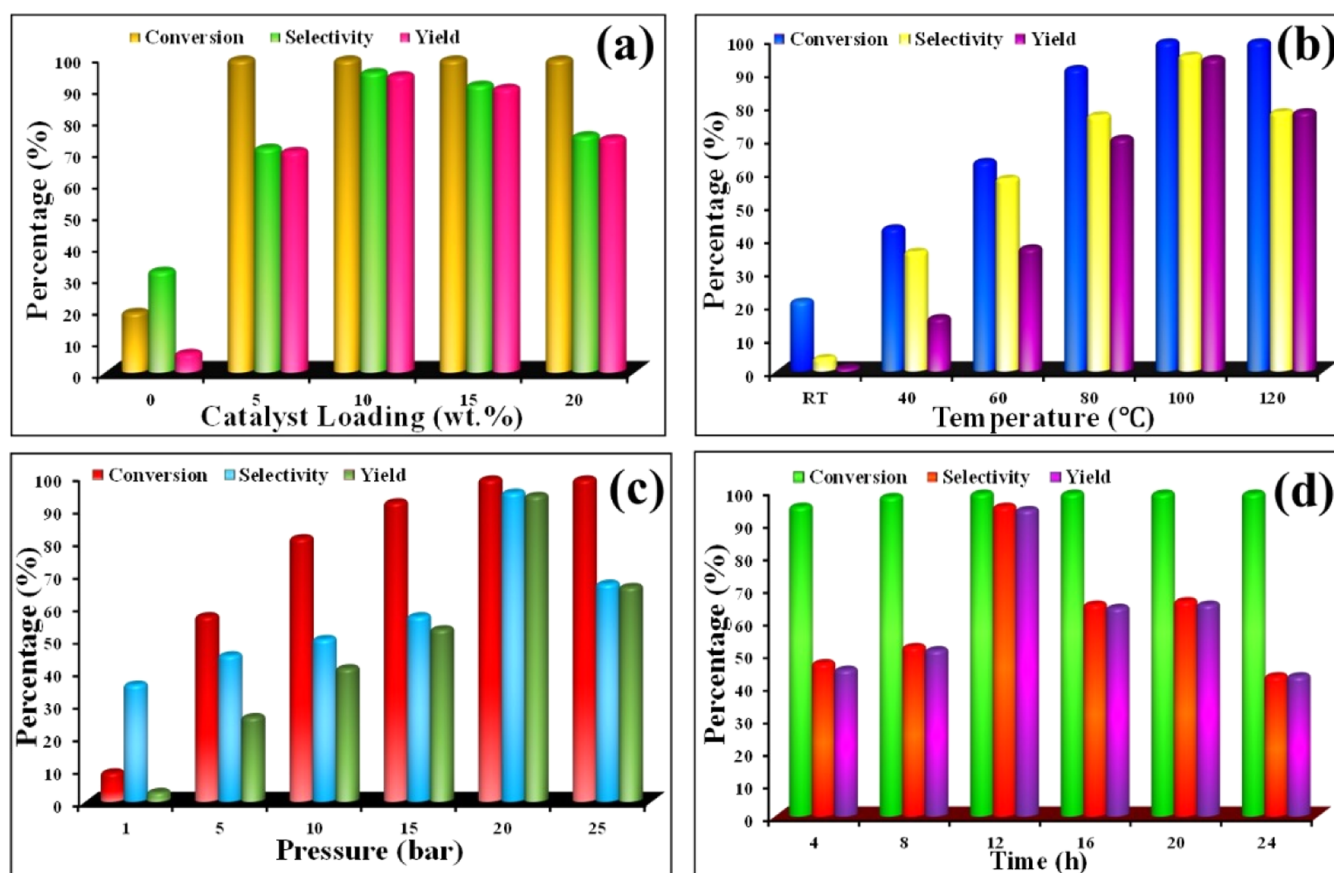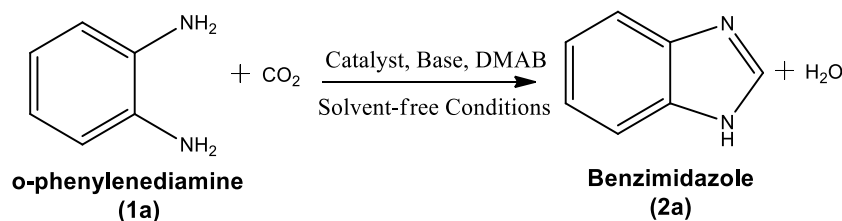
Figure 9. Influence of (a) catalyst loading, (b) reaction temperature, (c) CO_2 pressure (in bar), and (d) reaction time on CoMgCe TOS-catalyzed cyclization of CO_2 and **1a**.

small amount of the peak obtained at >600 °C was related to the adsorption of CO_2 on low coordination O^{2-} ions, leading to the formation of strongly basic sites.[45] Moreover, the corresponding quantitative estimation of these basic sites was calculated by integrating the area under the curves, and the obtained values are tabulated in Table 1. Hence, it can be said that, the basicity of the CoMgCe-TOS catalyst was tuned and possessed an appreciable number of basic sites when compared to single metal oxides. The overall NH_3 and CO_2-TPD results suggest that the introduction of different metals to prepare the trimetallic oxide catalyst could significantly enhance its acid–base properties.

3.9. Catalytic Activity. For initial investigations to explore the catalytic performance of the CoMgCe-TOS catalyst, the cyclization of gaseous CO_2 with solid *o*-phenylenediamine (**1a**) as the substrate was chosen as the benchmark reaction. These solvent-free reactions were performed with 10 wt % of catalyst, 0.5 mmol K_2CO_3 as base, and 3 mmol of DMAB as a reductant under 20 bar CO_2 pressure at 100 °C for 12 h to generate corresponding benzimidazole as the product (**2a**) in quantitative yields. As expected, no reaction occurred without any catalyst, DMAB, or base (Table 2, entry 1). Additionally, when reactions were individually performed in absence of the DMAB reductant, in the absence of the catalyst, and in the absence of the K_2CO_3 base, almost negligible (trace) yield of product **2a** was obtained (Table 2, entry 2–4). So far, mostly metal-based catalysts have been reported for the cyclization of CO_2 and **1a**.[20,65,66] Therefore, in addition to controlled studies, preliminary experiments were performed with different acidic and basic metal oxides. It is well-known that basic metal oxides

display high catalytic performance toward base-catalyzed reactions.[67] Based on the obtained CO_2-TPD results, it was confirmed that MgO and CeO_2 possessed good basic strengths. Therefore, pure MgO and CeO_2 were tested for the cyclization of CO_2 and **1a** synthesized by combustion of $Mg(NO_3)_2·6H_2O$ and $(NH_4)_2Ce(NO_3)_6$ in ethylene glycol, respectively. At 100 °C and 20 bar pressure, substrate **1a** with both MgO and CeO_2 showed excellent conversion of 99% after 12 h of reaction (Table 2, entries 5, 6). However, both exhibited lower selectivities toward product **2a**, possibly due to the rapid formation of inactive $MgCO_3$ and $Ce_2(CO_3)$ on the surface due to the dense presence of gaseous CO_2.[67] This observation clearly suggests that strong basic oxides proved to be inadequate for the cyclization reactions with CO_2.[67] In contrast, acidic Co_3O_4 catalyst displayed similar conversion (99%) of **1a**, however, an even lower selectivity toward **2a** was observed when compared to pure basic metal oxides (Table 2, entry 7). This implies that the presence of only acidic and only basic sites in the metal oxide catalysts might be responsible for the reduced selectivity and yield toward product **2a**. Hence, it can be presumed that the combination of acid–base properties in a catalytic system can provide a good number of catalytically active sites to enhance the selectivity toward product **2a**. As listed in Table 2, the three different combinations of trimetallic oxides in the ratio of (50:37.5:12.5) prepared by solution combustion synthesis using cobalt, magnesium, and cerium precursors, namely MgCoCe-TOS, CoMgCe-TOS, and CeCoMg-TOS, showed catalytic activities in the following order: CoMgCe-TOS > CeCoMg-TOS > MgCoCe-TOS (Table 2, entries 8–10). This suggested that the stoichiometric

Table 3. Influence on Cyclization of 1a and CO_2 Using Different Bases[a]

o-phenylenediamine (1a) + CO_2 → (Catalyst, Base, DMAB, Solvent-free Conditions) → Benzimidazole (2a) + H_2O

sr. no	catalyst (mg)	conversion[b] (%)	selectivity[b] (%)	yield[b] (%)
1	no base	99	27	26
2	Na_2CO_3	99	66	65
3	K_2CO_3	99	95	94
4	$CaCO_3$	88	59	52
5	Cs_2CO_3	99	87	86
6	KOH	97	75	73
7	^tBuOK	81	69	56
8	CH_3CO_2K	96	76	73

[a]Reaction conditions: 1 mmol OPD, 10 wt % (10 mg) CoMgCe catalyst, 0.5 mmol base, and 3 mmol DMAB, 100 °C, 20 bar CO_2 pressure, 12 h. [b]Conversion, yield, and selectivity of cyclic carbonate were determined using GC and GC−MS analyses.

combination of metals in the trimetallic oxides and the difference in their acid−base properties played important roles in catalyzing the reaction of CO_2 and **1a**. It is also important to mention that all the reactions concerning the cyclization of **1a** and CO_2 resulted in trace amounts of detectable byproducts.[23] Among the three trimetallic analogues, CoMgCe-TOS as a catalyst exhibited the best catalytic performance due to an optimum number of exposed acidic and basic sites and was hence selected as the optimum catalyst for investigating the influence of other reaction parameters.

3.9.1. Optimization of Reaction Parameters. With further progress toward optimizing reaction parameters, the influence of catalyst loading on the reaction was also investigated by keeping the other parameters constant. The obtained results are displayed in Figure 9a. As seen during initial catalytic studies, the yield of **2a** was negligible in the absence of catalyst, following which the increase in catalyst loading significantly affected the conversion of **1a**. For instance, on increasing the catalyst loading from 0 to 10 wt %, the conversion of **1a** increased remarkably to 99% and delivered an outstanding yield of 94% of product **2a**, suggesting the presence of an optimum number of active catalytic sites for the effective occurrence of the cyclization reaction.[23] When catalyst loading was decreased to 5 wt %, the yield of **2a** reduced to 70%, suggesting the availability of lesser number of active sites for interaction of **1a** with the CoMgCe-TOS catalyst. Further increases in catalyst loading to 15 and 20 wt %, provided product **2a** in less prominent yields of 91% and 75%, respectively. This decrease in yield could be attributed to the presence of excess catalyst which led to unavailability of catalytically active sites due to their poor dispersity in the reaction medium.[68] It is also worth mentioning that the porous scaffold-like framework of the CoMgCe-TOS catalyst exposed majority of the catalytically sites on the surface during the solution combustion synthesis process and resultantly exhibited excellent catalytic performance.

In further attempts to test the effectiveness of the reaction in the presence of the CoMgCe TOS catalyst, several reaction parameters, such as temperature, pressure, and time, were investigated. Upon considering reaction temperature, it was found that the catalytic performance increased linearly with

increase an in temperature from RT−100 °C, as shown in Figure 9b. The reaction performed at RT (25 °C) with 10 wt % of CoMgCe catalyst showed 21% conversion of **1a** and delivered product **2a** in trace amounts. An obvious increase in both conversion and selectivity was observed as the temperature was gradually elevated, suggesting the presence of a homogenized reaction environment for smooth mobilization of **1a** with the active species of the CoMgCe catalyst. Meanwhile, maximum conversion (99%) and selectivity (95%) toward product **2a** was obtained when the temperature was raised to 100 °C due to optimum activation energy and an increase in the number of effective collisions between **1a** and the CoMgCe catalyst.[69] As the temperature increased to 120 °C, the yield of product **2a** dropped to 78%, possibly due to overhydrogenation of **2a** which led to further formation of byproducts at elevated temperatures.[70] Hence, 100 °C was considered the optimum temperature when using CoMgCe TOSs as catalysts for the efficient conversion of **1a**.

The kinetics of cyclization reactions with CO_2 is greatly affected due to the diffusion of CO_2 in the reaction medium because CO_2 functions both as a reactant and solvent.[6,54] Therefore, the effect of CO_2 pressure on the cyclization reaction of CO_2 and **1a** was studied in the pressure range of 1 atm to 25 bar, while the other conditions remained constant, as shown in Figure 9c. Unfortunately, the existence of atmospheric pressure could not display improved reaction activity toward the formation of product **2a**. It was observed that the lower CO_2 pressure of 10 bar displayed remarkably increased conversion from 9 to 81% with 50% selective formation of product **2a**. Further, increasing the CO_2 pressure to 15 bar led to only a slight increase in selectivity (57%) toward **2a**. At a moderately high pressure of 20 bar CO_2 pressure, the cyclization reaction showed maximum conversion and selectivity of 99 and 95% respectively, with product **2a** in 94% yield at 100 °C after 12 h due to the excellent interaction of **1a** with the CoMgCe-TOS catalyst.[54] It can be presumed that at 20 bar, the concentrated CO_2 quickly consumed the stoichiometric amount of DMAB reductant, which hindered further reduction of reactant **1a** with DMAB and prevented further formation of byproducts.[71] However, beyond 20 bar pressure, there was substantial decrease in the selectivity and

yield of product **2a**, possibly because extremely high CO_2 pressure retarded the interaction between **1a** and CoMgCe catalyst due to the dilution effect.[54] This caused a lower concentration of **1a** in the vicinity of the catalytically active centers, thereby resulting in a decreased yield of **2a**.[54] Therefore, it can be concluded that effective pressure played a significant role toward selectivity of product **2a**.

Additionally, the influence of reaction time on CoMgCe TOS-catalyzed cyclization of CO_2 and **1a** is presented in Figure 9d. The conversion of **1a** increased smoothly with a gradual increase in the reaction time. The effect of reaction time showed that the yield of product **2a** increased from 45% in 4 h and reached the maximum conversion of 99% and yield of 94% toward product **2a** at 12 h. This indicates that increase in the reaction duration to 12 h promoted the cyclization of **1a** and CO_2 toward a chemical equilibrium state. Further prolonging the reaction time from 12 to 24 h did not result in any enhancement toward the cyclization of **1a** and CO_2. These results mean that the rate of formation of product **2a** decreased with an increase in the reaction time to 24 h. Hence, the above investigations indicate the optimal reaction time for the cyclization of **1a** and CO_2 was 12 h.

3.9.2. Influence of Different Bases. In continuation, different bases were scrutinized for the solvent-free cyclization of CO_2 and **1a** at 100 °C, 20 bar CO_2 pressure for 12 h, and the results are listed in Table 3. Experimental results suggested that the catalytic performance was remarkably affected toward the selective formation of **2a**, with different alkali and alkaline earth metal carbonates, namely Na_2CO_3, K_2CO_3, $CaCO_3$, and Cs_2CO_3.[72] Notably, using 10 wt % of CoMgCe catalyst and 3 mmol of DMAB as the reductant, the reaction did not proceed in the absence of base (Table 3, entry 1). In accordance with previous literature reports, K_2CO_3 as the base provided the highest yield of product **2a**, among the other carbonates listed (Table 3, entry 3). Surprisingly, catalytic activity with the use of Na_2CO_3 and $CaCO_3$ as bases was fairly low as compared to that of K_2CO_3 (Table 3, entries 2, 4 vs 3). However, Cs_2CO_3 as base showed satisfactory selectivity toward product **2a** and afforded a yield of 86%, due to the well-known "cesium effect" (Table 3, entry 5).[73] The difference in chemical reactivity of the different metal carbonates could be well attributed to the difference in basicities depending on the size of the metal cation present in carbonate salts.[73] Moreover, other potassium salts containing different anions such as hydroxide, acetate, and butoxide were also tested for the formation of product **2a**, which achieved lower yields than the carbonate anion (Table 3, entries 6−8). The use of strong base such as KOH resulted in a good conversion of 97% but showed a retarded selectivity of 75% possibly caused by the formation of HCO_3^- ions due to the presence of OH^- ion and gaseous CO_2.[74] Hence, based on the above results, K_2CO_3 was selected as the most optimal base for the cyclization of CO_2 and **1a** using the CoMgCe-TOS catalyst.

3.9.3. Influence of K_2CO_3 and DMAB Concentrations. Further, to see the encouraging influence of the amount of base on the cyclization of **1a** and CO_2, different amounts of K_2CO_3 were used. Interestingly, the cyclization reaction showed an excellent 99% conversion of **1a**, whereas the selectivity toward **2a** gradually increased as the amount of base was raised from 0.1 to 0.2 mmol (Table 4, entries 2, 3). On further increasing the amount of K_2CO_3 from 0.3 to 0.4 mmol, an almost similar selectivity toward product **2a** (Table 4, entries 4, 5). Notably, 94% yield could be obtained by

Table 4. Influence on Cyclization of 1a and CO_2 Using Different Amounts of K_2CO_3 and DMAB

sr. no	parameter	amount (mg)	conversion[c] (%)	selectivity[c] (%)	yield[c] (%)
1	amount of K_2CO_3[a]	no base	99	27	26
2		0.1	99	54	53
3		0.2	99	67	66
4		0.3	99	70	69
5		0.4	99	72	71
6		0.5	99	95	94
7		0.6	99	60	59
8	amount of DMAB[b]	no DMAB	27	11	3
9		1	45	28	13
10		2	51	58	30
11		3	99	95	94
12		4	99	86	86
13		5	99	64	63

[a]Reaction conditions: 1 mmol OPD, 10 wt % CoMgCe catalyst, K_2CO_3 base, and 3 mmol DMAB, 100 °C, 20 bar CO_2 pressure, 12 h. [b]Reaction conditions: 1 mmol OPD, 10 wt % CoMgCe catalyst, 0.5 mmol K_2CO_3 base, and DMAB, 100 °C, 20 bar CO_2 pressure, 12 h. [c]Conversion, yield, and selectivity of cyclic carbonate were determined using GC and GC−MS analyses.

increasing the amount of K_2CO_3 from 0.4 to 0.5 mmol (Table 4, entry 6), with no improvement in selectivity toward product **2a** with a further increase in the amount of K_2CO_3 to 0.6 mmol (Table 4, entry 7).

Further, the concentration of the reductant DMAB appeared to drastically influence the catalytic performance of CoMgCe TOSs toward the cyclization of **1a** and CO_2. Without DMAB, substrate **1a** showed a minor conversion and selectivity of 27 and 11%, respectively (Table 4, entry 8). When the concentration of DMAB was raised to 1 and 2 mmol, the yield of product **2a** increased gradually from 13 to 30% (Table 4, entries 9, 10). Next, 3 mmol of DMAB was screened, which provided the maximum conversion and selectivity of 99 and 95%, respectively, with an overall yield of 94% toward the desired product **2a** (Table 4, entry 11). Finally, upon further increase in the concentration of DMAB, no noticeable increase toward the selectivity of product **2a** was observed (Table 4, entry 12, 13). Thus, 0.5 mmol of K_2CO_3 and 3 mmol of DMAB appeared to be the optimum amount of base and reductant for the cyclization reactions of CO_2 and **1a**.

3.9.4. Substrate Scope. Enlightened by the worthy catalytic activity of the solvent-free CoMgCe-TOS-catalyzed system toward the synthesis of benzimidazole (**2**) from **1a** and CO_2 with DMAB as the reductant (Table 5, entry 1), the substrate scope was further expanded with electron-donating, electron-withdrawing, and other substituted aromatic amines under the optimized reaction conditions. The obtained results are shown in Table 5. Although *o*-phenylenediamines containing electron-withdrawing groups such as Cl in the 4th position were relatively inert to react with CO_2, which can be ascribed to the decrease in nucleophilicity of amino species, complete conversion and good yields (up to 88%) of 4-chloro benzimidazole were also obtained (Table 5, entry 2). The introduction of electron-donating ($-CH_3$) into the 4-position of **1a** could also afford corresponding 4-methyl benzimidazole with complete conversion and excellent yields (Table 5, entry 3). Interestingly, when 2-aminophenol and aminobenzenethiol

Table 5. Substrate Scope with the CoMgCe-TOS Catalyst for the Synthesis of Different N-Heterocyclic Compounds[a]

Sr. No	Substrate	Product	Conv.[b] (%)	Select.[b] (%)	Yield[b] (%)
1.	(o-phenylenediamine)	(benzimidazole)	99	95	94
2.	(4-chloro-1,2-benzenediamine)	(5-chlorobenzimidazole)	99	89	88
3.	(4-methyl-1,2-benzenediamine)	(5-methylbenzimidazole)	99	95	94
4.	(2-aminophenol)	(benzoxazole)	86	95	82
5.	(2-aminothiophenol)	(benzothiazole)	82	90	74

[a]Standard reaction conditions: 1 mmol amine, 10 wt % MgCoCe-TOS catalyst, 0.5 mmol K_2CO_3, and 3 mmol DMAB, 100 °C, 20 bar, 12 h.
[b]Conversion, yield, and selectivity of cyclic carbonate were determined using GC and GC−MS analyses.

Scheme 1. Possible Reaction Pathway for Cyclization of 1a and CO_2 Catalyzed by the CoMgCe-TOS Catalyst
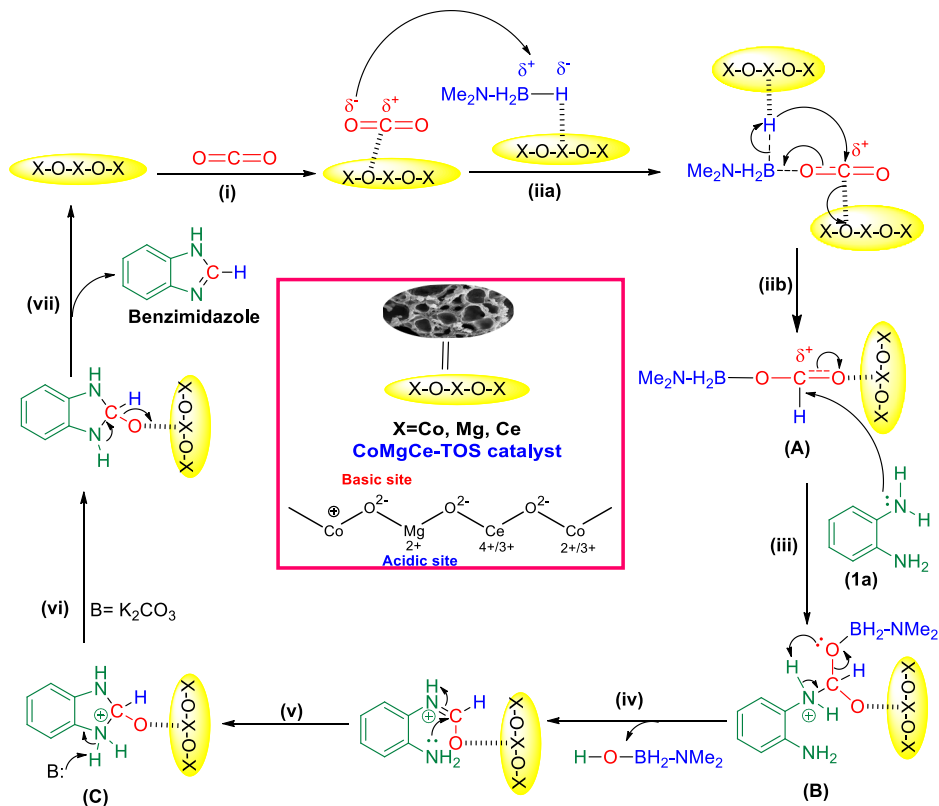
were used as substrates, 20 bar CO_2 pressure was enough for attaining counterpart N-containing benzoheterocyclic compounds, namely benzoxazole and benzothiazole, with 86 and 74% yield, respectively (Table 5, entries 4, 5). Although not optimized for these N-containing benzoheterocyclic compounds, the high yields indicate that the process is adaptable to other tandem syntheses of cyclic products. The above results illustrate that this low-cost and mild catalytic system is versatile for the reductive cyclization of various diamines with CO_2.

3.9.5. Plausible Reaction Mechanism. Reportedly, the development of benzimidazoles by employing *o*-phenylenediamines and CO_2 as reactants in the presence of reducing
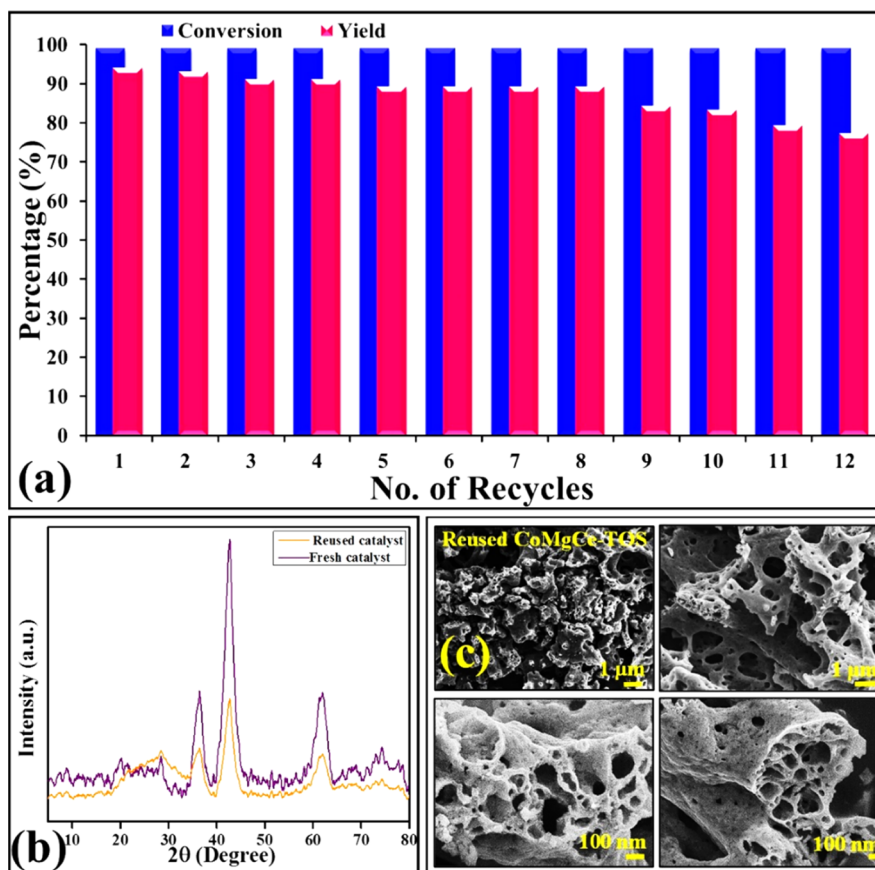
Figure 10. (a) Recyclability Studies for cyclization of CO_2 and **1a** into benzimidazole catalyzed by the CoMgCe-TOS catalyst. (b) XRD analysis and (c) FE-SEM analysis of the reused CoMgCe-TOS catalyst after 12th recycle.

agents requires the presence of both acidic as well as basic sites.[23] According to Dyson et al., catalysts for benzimidazole production should comprise both acidic and basic sites. The first N-formylation step during the tandem synthesis of benzimidazole is base-catalyzed, whereas the subsequent cyclization step is mostly Lewis acid-catalyzed.[23] Therefore, the Lewis acid strength of the catalyst plays an essential role in product selectivity.[23] Additionally, the formation of benzimidazoles under ambient reaction conditions relies heavily on the combined effects of acid−base strength, lattice O^{2-} density to determine selectivity toward the desired benzimidazole product.[23,75] Based on the NH_3/CO_2-TPD (acidic/basic sites), H_2-TPR (metal−metal interaction), XPS analysis (lattice O^{2-} sites), and experimental results, a plausible reaction mechanism was proposed for the cyclization of **1a** and CO_2 to benzimidazole catalyzed by the CoMgCe-TOS catalyst.
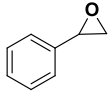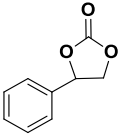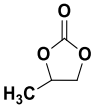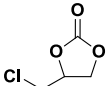
As per the previous literature reports for CO_2-based reactions, it can be said that the Lewis basic sites of the catalyst aid in the easy activation of the acidic CO_2 reactant.[6] As confirmed from the deconvoluted O 1s XPS spectra, the CoMgCe-TOS catalyst showed the presence of lattice O^{2-} species. Hence, as shown in Scheme 1, it can be proposed that the reaction was initiated by the adsorption and consequent activation of CO_2 through the Lewis basic O^{2-} sites of CoMgCe-TOS catalyst (step (i)).[6,76] Following this, DMAB was activated by hydrogen bonding (activated B−H bond) with the metallic Lewis acidic sites of the catalyst (step (iia)). Further, the C−O bond of activated CO_2 was inserted between

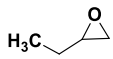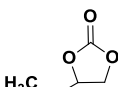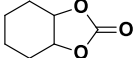the activated B−H bond of DMAB (step (iib)) to generate an intermediate (A).[66] Subsequently, in step (iii), the electronically rich "N" atom of reactant (**1a**) attacked the electron-deficient carbon atom of CO_2 in intermediate (A) to generate carbamate intermediate (B).[76] This was followed by elimination of side product in the form of hydroxy-N,N-dimethylamine borane (OH-BH_2NMe_2) to generate a N-(2-aminophenyl)formamide intermediate (step (iv)).[66,76] Next, the N-(2-aminophenyl)formamide intermediate underwent intramolecular cyclization to form a cyclized intermediate (C) (step (v)).[76] Further, the base (K_2CO_3) enhanced the rate of reaction by promoting H^+ abstraction (step (vi)) and neutralizing the charge on the "N" atom, followed by aromatization at a higher rate to give the desired cyclic product, benzimidazole.[75] The benzimidazole product thus formed gets desorbed from the catalyst surface, whereas the lattice O^{2-} sites of the CoMgCe-TOS catalyst combine with the protons (H^+) from base and electrons released from the metallic species reduction to form water, thereby undergoing dehydration (step (vii)) and resulting in the closure of the catalytic cycle.[75]

3.9.6. Recyclability Studies and Characterization after Reuse. The efficiency and reusability of the heterogeneous catalysts determine their adaptability toward industrial applications.[6,22] The reusability of CoMgCe-TOS catalyst was determined by performing the catalytic runs for the cyclization of CO_2 and **1a** for the synthesis of benzimidazole using 1 mmol OPD, 10 wt % CoMgCe-TOS catalyst, 0.5 mmol K_2CO_3 base, 3 mmol DMAB, 100 °C, 20 bar CO_2 pressure,

Table 6. CoMgCe-TOS-Catalyzed Synthesis of Cyclic Carbonates by Using Epoxides and CO_2[a]

Sr. No.	Substrate	Product	Conv.[b] (%)	Select.[b] (%)	Yield[b] (%)
1.			94	92	86
2.			100	99	99
3.			98	94	92
4.			93	93	85
5.			81	79	64

[a]Standard reaction conditions: 8.3 mmol epoxide, 10 wt % MgCoCe-TOS catalyst, and 0.2 mmol TBAI, 100 °C, 20 bar, 12 h. [b]Conversion, yield, and selectivity of cyclic carbonate were determined using GC−MS analyses.

and 12 h considered as optimized reaction conditions. Subsequently, the catalyst was recovered by a simple filtration technique and washed with ethanol, followed by drying in an oven after the completion of each cycle. It was further used for subsequent cycles under the optimized reaction conditions. The recyclability results are picturized in Figure 10a. It was observed that the CoMgCe-TOS catalyst yielded better results for a fair amount of runs, and it could be reused for 12 consecutive cycles. There was not much loss in the activity of CoMgCe-TOS catalyst toward the cyclization of 1a and CO_2 to obtain benzimidazole. At the end of the 6th recycle, the conversion of 1a remained at 99%, whereas the selectivity of benzimidazole decreased to 89%. Correspondingly at the end of the 12th cycle, the conversion of 1a remained the same, whereas there was a slight decrease of selectivity toward benzimidazole of around 17% considering the 1st cycle (95 to 78%). The drop in selectivity toward benzimidazole could be attributed to the blockage of pores in the CoMgCe-TOS catalyst by stuck organic molecules and the adsorption of moisture on the surface of the catalyst during the consecutive recycles.[6,22]

Furthermore, the morphological and chemical changes in the reused CoMgCe-TOS catalyst were examined using XRD and FE-SEM analyses. The XRD diffractogram of the reused CoMgCe-TOS catalyst (Figure 10b) shows that all the peaks in the reused CoMgCe-TOS catalyst matched well with the characteristic peaks observed in the fresh catalyst. Furthermore, the scaffold-like morphology was well-preserved in the reused CoMgCe-TOS catalyst, as shown in Figure 10c, with no obvious morphological changes. The EDX and mapping and analysis of the reused CoMgCe-TOS catalyst shows the presence of Co, Mg, Ce, and O elements similar to those present in the pristine catalyst. Therefore, it can be concluded that the chemical and structural integrity of the CoMgCe-TOS

catalyst was maintained throughout all cycles of the reusability studies and confirmed by the above findings. Hence, the CoMgCe-TOS catalyst can be categorized as a highly efficient, reusable, and robust catalyst for the fixation of CO_2 for organic transformations.

3.10. CoMgCe-TOS-Catalyzed Conversion of Epoxides and CO_2 to Cyclic Carbonates. To expand and display the catalytic versatility of the CoMgCe-TOS catalyst, it was further used for the conversion of CO_2 into epoxides to form cyclic carbonates. Cyclic carbonates are used in a wide range of applications, namely as solvents, as electrolytes in Li-ion batteries, in the production of fine chemicals, and as biomedicines to name a few. Nowadays, much focus is given on the synthesis of catalysts which favorably yield cyclic carbonates upon cycloaddition of epoxides and CO_2. Though enormous work has been done in this regard, there still lies scope for the development of catalysts which can efficiently yield cyclic carbonates under greener reaction conditions. Also, the cycloaddition reaction between CO_2 and epoxides to yield cyclic carbonates is considered one of the important reactions as it employs CO_2 as nontoxic reactant and is a 100% atom-economical process. The present work is the first of the kind report where TOSs synthesized by solution combustion processes have been used for the cyclization of CO_2 and epoxides to produce cyclic carbonates. Additionally, the cycloaddition reactions were performed under the same conditions by employing 10 wt % of CoMgCe catalyst, heating at 100 °C, 20 bar CO_2 pressure for 12 h. The results obtained for the cycloaddition reactions are presented in Table 6.

For example, on reaction with CO_2, propylene oxide showed 95% conversion and 59% selectivity toward propylene carbonate (55% yield) in presence of 0.5 mmol of K_2CO_3 as a base. By changing the base to TBAI and varying its amount, complete conversion and an increase in selectivity to 99%

when using 0.2 mmol of TBAI were observed. To support the dual catalytic property of CoMgCe-TOS catalyst, it can be observed from the characterization studies such as, BET, XRD, FE-SEM, NH_3/CO_2 TPD, and H_2-TPR that the catalyst exhibited better surface area, moderate crystallinity, a porous nature, the presence of both types of acidic as well as basic sites, and strong metal−metal interaction. These characteristic features enabled the CoMgCe-TOS catalyst to give better yield of propylene carbonate. The CoMgCe-TOS catalyst displayed bifunctional acid−base characteristics, wherein the Lewis acidic metallic sites helped in the activation of epoxide and the basic oxygen sites helped in the adsorption and activation of CO_2.[6] Further, the ring opening of the epoxide was stabilized by the presence of base (TBAI). Moreover, the CoMgCe-TOS catalyst was also subjected to various substrates of epoxide to check the efficacy of the catalyst toward CO_2 conversion to form respective cyclic carbonates. Notably, the reaction with styrene oxide under the same reaction conditions in the presence of 0.2 mmol of TBAI resulted in 94% conversion of styrene oxide and 92% selectivity toward styrene carbonate (86% yield). The reaction with cyclohexene oxide yielded 81% conversion with 79% selectivity toward cyclohexene carbonate (64% yield). This indicated that the catalytic activity was affected upon the increase in steric hindrance from the substituents on the side chain of the epoxides.[6] Further, the effect of the electron-withdrawing groups and electron-donating groups present in the side chain of epoxide ring was also tested. It was revealed that the presence of an electron-withdrawing (chloromethyl) group in the epichlorohydrin assisted in the ring opening of the epichlorohydrin; as a result, 98% conversion of epichlorohydrin, 94% selectivity toward chloropropylene carbonate, and 92% yield were obtained. The presence of electron-donating groups in butylene oxide did not show much variation in the respective yields and obtained a conversion of 93% with 93% selectivity toward butylene carbonate (85% yield). This showed that the electron-donating groups did not have much influence on the catalytic activity.

4. CONCLUSIONS

In conclusion, this work focuses on the development of mesoporous TOSs for the solvent-free valorization of CO_2 into various value-added products. Innovative CoMgCe-TOS as heterogeneous catalysts were developed using a cost-effective, quick, and energy-saving one-step solution combustion synthesis strategy using metal nitrate precursors as oxidizers and ethylene glycol as the fuel system at lower temperatures, which follows the principles of sustainable chemistry. The microstructure of CoMgCe-TOS catalyst showed a highly ordered 3D-porous scaffold-like architecture with a large number of homogeneously distributed pores. The generation of these interconnected pores was primarily governed by the evolution of nitrate ions from the metal precursors during the self-combustion process. This resulted in an appreciable surface area, acid−base cooperative sites, and a larger pore volume in the catalyst. The thoroughly characterized CoMgCe-TOS catalyst was applied as a multitasking heterogeneous catalyst for the transformation of CO_2 into value-added products through a range of two different reactions, namely (i) conversion of *o*-phenylenediamine and CO_2 to benzimidazoles and (ii) conversion of epoxides and CO_2 to cyclic carbonates. In the presence of 3 mmol DMAB instead of harmful substrates and flammable H_2 gas as the reductant,

benzimidazoles were obtained in 95% selectivity and 94% yield using 10 wt % CoMgCe-TOS as the catalyst at 100 °C, 20 bar, and 12 h of reaction time. Different experimental conditions, such as variation in the catalyst loading, K_2CO_3 loading, DMAB loading, temperature, pressure, and time, were investigated. Besides the production of N-containing heterocycles, the CoMgCe-TOS catalyst was also very active for the synthesis of cyclic carbonates from various internal and terminal epoxides and CO_2 in the presence of TBAI as the base under similar reaction conditions. Interestingly, the CoMgCe-TOS catalyst could be easily recycled for 12 consecutive cycles without significant loss in activity. Based on the results obtained, a plausible mechanism was also predicted in order to support the performed reactions. The results presented in this research effort are a proof of concept for the first successful application of trimetallic oxide prepared using an energy-saving one-step solution combustion synthesis strategy at lower temperatures as a versatile heterogeneous catalytic system for the synthesis of benzimidazoles and organic carbonates, which can be easily adapted for scale-up applications.

■ AUTHOR INFORMATION

Corresponding Author

Arvind H. Jadhav − *Centre for Nano and Material Science, JAIN University, Bangalore 562112 Karnataka, India;* ⊙ orcid.org/0000-0002-9128-1981; Email: j.arvind@jainuniversity.ac.in, jadhav.ah@gmail.com

Authors

Divya Prasad − *Centre for Nano and Material Science, JAIN University, Bangalore 562112 Karnataka, India; Department of Chemical and Biomolecular Engineering, University of California Berkeley, Berkeley, California 94720, United States*

Puneethkumar M. Srinivasappa − *Centre for Nano and Material Science, JAIN University, Bangalore 562112 Karnataka, India*

Navya Anna Raju − *Centre for Nano and Material Science, JAIN University, Bangalore 562112 Karnataka, India*

Akshaya K. Samal − *Centre for Nano and Material Science, JAIN University, Bangalore 562112 Karnataka, India*

Complete contact information is available at:
https://pubs.acs.org/10.1021/acs.energyfuels.2c03513

Notes

The authors declare no competing financial interest.

■ REFERENCES

(1) Aresta, M.; Dibenedetto, A.; Angelini, A. Catalysis for the Valorization of Exhaust Carbon: From CO_2 to Chemicals, Materials, and Fuels. Technological Use of CO_2. *Chem. Rev.* **2014**, *114*, 1709−1742.

(2) Centi, G.; Quadrelli, E. A.; Perathoner, S. Catalysis for CO_2 Conversion: A Key Technology for Rapid Introduction of Renewable Energy in the Value Chain of Chemical Industries. *Energy Environ. Sci.* **2013**, *6*, 1711−1731.

(3) Liu, Q.; Wu, L.; Jackstell, R.; Beller, M. Using Carbon Dioxide as a Building Block in Organic Synthesis. *Nat. Commun.* **2015**, *6*, 5933.

(4) Song, C. Global Challenges and Strategies for Control, Conversion and Utilization of CO_2 for Sustainable Development Involving Energy, Catalysis, Adsorption and Chemical Processing. *Catal. Today* **2006**, *115*, 2−32.

(5) North, M. What Is CO_2? Thermodynamics, Basic Reactions and Physical Chemistry. *Carbon Dioxide Utilisation*; Elsevier, 2015; pp 3−17.

(6) Prasad, D.; Patil, K. N.; Dateer, R. B.; Kim, H.; Nagaraja, B. M.; Jadhav, A. H. Basicity Controlled $MgCo_2O_4$ Nanostructures as Catalyst for Viable Fixation of CO_2 into Epoxides at Atmospheric Pressure. *Chem. Eng. J.* **2021**, *405*, 126907.

(7) Sharma, R. K.; Gaur, R.; Yadav, M.; Goswami, A.; Zbořil, R.; Gawande, M. B. An Efficient Copper-Based Magnetic Nanocatalyst for the Fixation of Carbon Dioxide at Atmospheric Pressure. *Sci. Rep.* **2018**, *8*, 1901.

(8) Subramanian, S.; Song, Y.; Kim, D.; Yavuz, C. T. Redox and Nonredox CO_2 Utilization: Dry Reforming of Methane and Catalytic Cyclic Carbonate Formation. *ACS Energy Lett.* **2020**, *5*, 1689−1700.

(9) Wang, W.-H.; Himeda, Y.; Muckerman, J. T.; Manbeck, G. F.; Fujita, E. CO_2 Hydrogenation to Formate and Methanol as an Alternative to Photo-and Electrochemical CO_2 Reduction. *Chem. Rev.* **2015**, *115*, 12936−12973.

(10) Sharma, P.; Kumar, S.; Tomanec, O.; Petr, M.; Zhu Chen, J.; Miller, J. T.; Varma, R. S.; Gawande, M. B.; Zbořil, R. Carbon Nitride-based Ruthenium Single Atom Photocatalyst for CO_2 Reduction to Methanol. *Small* **2021**, *17*, 2006478.

(11) Bobbink, F. D.; Das, S.; Dyson, P. J. N-Formylation and N-Methylation of Amines Using Metal-Free N-Heterocyclic Carbene Catalysts and CO_2 as Carbon Source. *Nat. Protoc.* **2017**, *12*, 417−428.

(12) Zhang, Z.; Sun, Q.; Xia, C.; Sun, W. CO_2 as a C1 Source: $B(C_6F_5)_3$-Catalyzed Cyclization of o-Phenylene-Diamines To Construct Benzimidazoles in the Presence of Hydrosilane. *Org. Lett.* **2016**, *18*, 6316−6319.

(13) Navarrete-Vázquez, G.; Cedillo, R.; Hernández-Campos, A.; Yépez, L.; Hernández-Luis, F.; Valdez, J.; Morales, R.; Cortés, R.; Hernández, M.; Castillo, R. Synthesis and Antiparasitic Activity of 2-(Trifluoromethyl)Benzimidazole Derivatives. *Bioorg. Med. Chem. Lett.* **2001**, *11*, 187−190.

(14) Wright, J. B. The Chemistry of the Benzimidazoles. *Chem. Rev.* **2002**, *48*, 397−541.

(15) Gao, X.; Yu, B.; Mei, Q.; Yang, Z.; Zhao, Y.; Zhang, H.; Hao, L.; Liu, Z. Atmospheric CO_2 Promoted Synthesis of N-Containing Heterocycles over $B(C6F5)3$ Catalyst. *New J. Chem.* **2016**, *40*, 8282−8287.

(16) Sheykhan, M.; Mohammadquli, M.; Heydari, A. A New and Green Synthesis of Formamidines by γ-$Fe_2O_3@SiO_2$−HBF_4 Nanoparticles as a Robust and Magnetically Recoverable Catalyst. *J. Mol. Struct.* **2012**, *1027*, 156−161.

(17) Yu, L.; Zhang, Q.; Li, S.-S.; Huang, J.; Liu, Y.-M.; He, H.-Y.; Cao, Y. Gold-Catalyzed Reductive Transformation of Nitro Compounds Using Formic Acid: Mild, Efficient, and Versatile. *ChemSusChem* **2015**, *8*, 3029−3035.

(18) Sharma, S.; Sharma, A.; Yamini; Das, P. Supported Rhodium (Rh@PS) Catalyzed Benzimidazoles Synthesis Using Ethanol/Methanol as C_2H_3/CH Source. *Adv. Synth. Catal.* **2019**, *361*, 67−72.

(19) Yu, B.; Zhang, H.; Zhao, Y.; Chen, S.; Xu, J.; Huang, C.; Liu, Z. Cyclization of O-Phenylenediamines by CO_2 in the Presence of H_2 for the Synthesis of Benzimidazoles. *Green Chem.* **2013**, *15*, 95−99.

(20) Saptal, V. B.; Sasaki, T.; Bhanage, B. M. Ru@PsIL-Catalyzed Synthesis of N -Formamides and Benzimidazole by using Carbon Dioxide and Dimethylamine Borane. *ChemCatChem* **2018**, *10*, 2593−2600.

(21) Jacquet, O.; Das Neves Gomes, C.; Ephritikhine, M.; Cantat, T. Complete Catalytic Deoxygenation of CO_2 into Formamidine Derivatives. *ChemCatChem* **2013**, *5*, 117−120.

(22) Patil, K. N.; Prasad, D.; Bhagyashree; Manoorkar, V. K.; Nabgan, W.; Nagaraja, B. M.; Jadhav, A. H. Engineered Nano-Foam of Tri-Metallic (FeCuCo) Oxide Catalyst for Enhanced Hydrogen Generation via $NaBH_4$ Hydrolysis. *Chemosphere* **2021**, *281*, 130988.

(23) Hulla, M.; Nussbaum, S.; Bonnin, A. R.; Dyson, P. J. The Dilemma between Acid and Base Catalysis in the Synthesis of Benzimidazole from O-Phenylenediamine and Carbon Dioxide. *Chem. Commun.* **2019**, *55*, 13089−13092.

(24) Liu, X.; Long, Q.; Jiang, C.; Zhan, B.; Li, C.; Liu, S.; Zhao, Q.; Huang, W.; Dong, X. Facile and Green Synthesis of Mesoporous Co_3O_4 Nanocubes and Their Applications for Supercapacitors. *Nanoscale* **2013**, *5*, 6525−6529.

(25) Shishido, T.; Sameshima, H.; Takehira, K. Methanol Decomposition to Synthesis Gas over Supported Pd Catalysts Prepared from Hydrotalcite Precursors. *Top. Catal.* **2003**, *22*, 261−269.

(26) Wang, Y.; Liu, B.; Huang, K.; Zhang, Z. Aerobic Oxidation of Biomass-Derived 5-(Hydroxymethyl)furfural into 2,5-Diformylfuran Catalyzed by the Trimetallic Mixed Oxide (Co-Ce-Ru). *Ind. Eng. Chem. Res.* **2014**, *53*, 1313−1319.

(27) Choudhary, V. R.; Mondal, K. C.; Choudhary, T. V. Oxy-Methane Reforming over High Temperature Stable $NiCoMgCeO_x$ and $NiCoMgO_x$ Supported on Zirconia−Haffnia Catalysts: Accelerated Sulfur Deactivation and Regeneration. *Catal. Commun.* **2007**, *8*, 561−564.

(28) Al-Doghachi, F. A. J.; Rashid, U.; Zainal, Z.; Saiman, M. I.; Taufiq Yap, Y. H. Influence of Ce_2O_3 and CeO_2 Promoters on Pd/MgO Catalysts in the Dry-Reforming of Methane. *RSC Adv.* **2015**, *5*, 81739−81752.

(29) Ramadass, S. K.; Perumal, S.; Gopinath, A.; Nisal, A.; Subramanian, S.; Madhan, B. Sol-Gel Assisted Fabrication of Collagen Hydrolysate Composite Scaffold: A Novel Therapeutic Alternative to the Traditional Collagen Scaffold. *ACS Appl. Mater. Interfaces* **2014**, *6*, 15015−15025.

(30) Kumar, R.; Youssry, S. M.; Soe, H. M.; Abdel-Galeil, M. M.; Kawamura, G.; Matsuda, A. Honeycomb-like Open-Edged Reduced-Graphene-Oxide-Enclosed Transition Metal Oxides (NiO/Co_3O_4) as Improved Electrode Materials for High-Performance Supercapacitor. *J. Energy Storage* **2020**, *30*, 101539.

(31) Khort, A.; Romanovski, V.; Lapitskaya, V.; Kuznetsova, T.; Yusupov, K.; Moskovskikh, D.; Haiduk, Y.; Podbolotov, K. Graphene@Metal Nanocomposites by Solution Combustion Synthesis. *Inorg. Chem.* **2020**, *59*, 6550−6565.

(32) Song, G.; Zhu, X.; Chen, R.; Liao, Q.; Ding, Y.-D.; Chen, L. Influence of the Precursor on the Porous Structure and CO_2 Adsorption Characteristics of MgO. *RSC Adv.* **2016**, *6*, 19069−19077.

(33) He, H.; Dai, H. X.; Ng, L. H.; Wong, K. W.; Au, C. T. Pd-, Pt-, and Rh-Loaded $Ce_{0.6}Zr_{0.35}Y_{0.05}O_2$ Three-Way Catalysts: An Investigation on Performance and Redox Properties. *J. Catal.* **2002**, *206*, 1−13.

(34) Li, J.; Lu, G.; Wu, G.; Mao, D.; Wang, Y.; Guo, Y. Promotional Role of Ceria on Cobaltosic Oxide Catalyst for Low-Temperature CO Oxidation. *Catal. Sci. Technol.* **2012**, *2*, 1865−1871.

(35) Elkhalifa, E. A.; Friedrich, H. B. Magnesium Oxide as a Catalyst for the Dehydrogenation of N-Octane. *Arabian J. Chem.* **2018**, *11*, 1154−1159.

(36) Smith, L. R.; Sainna, M. A.; Douthwaite, M.; Davies, T. E.; Dummer, N. F.; Willock, D. J.; Knight, D. W.; Catlow, C. R. A.; Taylor, S. H.; Hutchings, G. J. Gas Phase Glycerol Valorization over Ceria Nanostructures with Well-Defined Morphologies. *ACS Catal.* **2021**, *11*, 4893−4907.

(37) Watanabe, S.; Ma, X.; Song, C. Characterization of Structural and Surface Properties of Nanocrystalline TiO_2− CeO_2 Mixed Oxides by XRD, XPS, TPR, and TPD. *J. Phys. Chem. C* **2009**, *113*, 14249−14257.

(38) Laguna, O. H.; Centeno, M. Á.; Romero-Sarria, F.; Odriozola, J. A. Oxidation of CO over Gold Supported on Zn-Modified Ceria Catalysts. *Catal. Today* **2011**, *172*, 118−123.

(39) Long, G.; Chen, M.; Li, Y.; Ding, J.; Sun, R.; Zhou, Y.; Huang, X.; Han, G.; Zhao, W. One-Pot Synthesis of Monolithic Mn-Ce-Zr Ternary Mixed Oxides Catalyst for the Catalytic Combustion of Chlorobenzene. *Chem. Eng. J.* **2019**, *360*, 964−973.

(40) Habibi, N.; Arandiyan, H.; Rezaei, M. Mesoporous MgO· Al₂O₃ Nanopowder-Supported Meso−Macroporous Nickel Catalysts: A New Path to High-Performance Biogas Reforming for Syngas. *RSC Adv.* **2016**, *6*, 29576−29585.

(41) Zhang, F.; Liu, Z.; Zhang, S.; Akter, N.; Palomino, R. M.; Vovchok, D.; Orozco, I.; Salazar, D.; Rodriguez, J. A.; Llorca, J.; Lee, J.; Kim, D.; Xu, W.; Frenkel, A. I.; Li, Y.; Kim, T.; Senanayake, S. D. In Situ Elucidation of the Active State of Co−CeOₓ Catalysts in the Dry Reforming of Methane: The Important Role of the Reducible Oxide Support and Interactions with Cobalt. *ACS Catal.* **2018**, *8*, 3550−3560.

(42) Lucrédio, A. F.; Tremiliosi Filho, G.; Assaf, E. M. Co/Mg/Al Hydrotalcite-Type Precursor, Promoted with La and Ce, Studied by XPS and Applied to Methane Steam Reforming Reactions. *Appl. Surf. Sci.* **2009**, *255*, 5851−5856.

(43) Al-Swai, B. M.; Osman, N.; Alnarabiji, M. S.; Adesina, A. A.; Abdullah, B. Syngas Production via Methane Dry Reforming over Ceria-Magnesia Mixed Oxide-Supported Nickel Catalysts. *Ind. Eng. Chem. Res.* **2018**, *58*, 539−552.

(44) McNulty, D.; Geaney, H.; O'Dwyer, C. Carbon-Coated Honeycomb Ni-Mn-Co-O Inverse Opal: A High Capacity Ternary Transition Metal Oxide Anode for Li-Ion Batteries. *Sci. Rep.* **2017**, *7*, 42263.

(45) Podila, S.; Driss, H.; Zaman, S. F.; Ali, A. M.; Al-Zahrani, A. A.; Daous, M. A.; Petrov, L. A. Mgfe and Mg−Co−Fe Mixed Oxides Derived from Hydrotalcites: Highly Efficient Catalysts for COₓ Free Hydrogen Production from NH₃. *Int. J. Hydrogen Energy* **2020**, *45*, 873−890.

(46) Larachi, F.; Pierre, J.; Adnot, A.; Bernis, A. Ce 3d XPS Study of Composite CeₓMn₁₋ₓO₂₋ᵧ Wet Oxidation Catalysts. *Appl. Surf. Sci.* **2002**, *195*, 236−250.

(47) Bêche, E.; Charvin, P.; Perarnau, D.; Abanades, S.; Flamant, G. Ce 3d XPS Investigation of Cerium Oxides and Mixed Cerium Oxide (CeₓTiᵧOᵤ). *Surf. Interface Anal.* **2008**, *40*, 264−267.

(48) Wang, A. Q.; Punchaipetch, P.; Wallace, R. M.; Golden, T. D. X-Ray Photoelectron Spectroscopy Study of Electrodeposited Nanostructured CeO₂ Films. *J. Vac. Sci. Technol., B: Microelectron. Nanometer Struct.–Process., Meas., Phenom.* **2003**, *21*, 1169−1175.

(49) Luisetto, I.; Tuti, S.; Battocchio, C.; Lo Mastro, S.; Sodo, A. Ni/CeO₂−Al2O₃ Catalysts for the Dry Reforming of Methane: The Effect of CeAlO₃ Content and Nickel Crystallite Size on Catalytic Activity and Coke Resistance. *Appl. Catal., A* **2015**, *500*, 12−22.

(50) Zhang, L. H.; Li, F.; Evans, D. G.; Duan, X. Cu−Zn−(Mn)−(Fe)−Al Layered Double Hydroxides and Their Mixed Metal Oxides: Physicochemical and Catalytic Properties in Wet Hydrogen Peroxide Oxidation of Phenol. *Ind. Eng. Chem. Res.* **2010**, *49*, 5959−5968.

(51) Shanmugavani, A.; Selvan, R. K. Improved Electrochemical Performances of CuCo₂O₄/CuO Nanocomposites for Asymmetric Supercapacitors. *Electrochim. Acta* **2016**, *188*, 852−862.

(52) Yan, T.; Bing, W.; Xu, M.; Li, Y.; Yang, Y.; Cui, G.; Yang, L.; Wei, M. Acid-base sites synergistic catalysis over Mg-Zr-Al mixed metal oxide toward synthesis of diethyl carbonate. *RSC Adv.* **2018**, *8*, 4695−4702.

(53) Bhanushali, J. T.; Kainthla, I.; Keri, R. S.; Nagaraja, B. M. Catalytic Hydrogenation of Benzaldehyde for Selective Synthesis of Benzyl Alcohol: A Review. *ChemistrySelect* **2016**, *1*, 3839−3853.

(54) Prasad, D.; Patil, K. N.; Bhanushali, J. T.; Nagaraja, B. M.; Jadhav, A. H. Sustainable Fixation of CO 2 into Epoxides to Form Cyclic Carbonates Using Hollow Marigold CuCo₂O₄ Spinel Microspheres as a Robust Catalyst. *Catal. Sci. Technol.* **2019**, *9*, 4393−4412.

(55) Li, G.; Zhang, C.; Wang, Z.; Huang, H.; Peng, H.; Li, X. Fabrication of Mesoporous Co₃O₄ Oxides by Acid Treatment and Their Catalytic Performances for Toluene Oxidation. *Appl. Catal., A* **2018**, *550*, 67−76.

(56) Huang, X.; Men, Y.; Wang, J.; An, W.; Wang, Y. Highly Active and Selective Binary MgO−SiO₂ Catalysts for the Production of 1, 3-Butadiene from Ethanol. *Catal. Sci. Technol.* **2017**, *7*, 168−180.

(57) Zhang, D.; Zhang, L.; Shi, L.; Fang, C.; Li, H.; Gao, R.; Huang, L.; Zhang, J. In Situ Supported MnOₓ−CeOₓ on Carbon Nanotubes for the Low-Temperature Selective Catalytic Reduction of NO with NH₃. *Nanoscale* **2013**, *5*, 1127−1136.

(58) Wu, Y.; Song, X.; Xu, S.; Chen, Y.; Oderinde, O.; Gao, L.; Wei, R.; Xiao, G. Chemical Fixation of CO₂ into Cyclic Carbonates Catalyzed by Bimetal Mixed MOFs: The Role of the Interaction between Co and Zn. *Dalton Trans.* **2020**, *49*, 312−321.

(59) Yong, J.; Luan, X.; Dai, X.; Zhang, X.; Yang, Y.; Zhao, H.; Cui, M.; Ren, Z.; Nie, F.; Huang, X. Alkaline-Etched NiMgAl Trimetallic Oxide-Supported KMoS-Based Catalysts for Boosting Higher Alcohol Selectivity in CO Hydrogenation. *ACS Appl. Mater. Interfaces* **2019**, *11*, 19066−19076.

(60) Gao, Y.; Zhang, Z.; Wu, J.; Yi, X.; Zheng, A.; Umar, A.; O'Hare, D.; Wang, Q. Comprehensive Investigation of CO₂ Adsorption on Mg−Al−CO₃ LDH-Derived Mixed Metal Oxides. *J. Mater. Chem. A* **2013**, *1*, 12782−12790.

(61) Manríquez-Ramírez, M.; Gómez, R.; Hernández-Cortez, J. G.; Zúñiga-Moreno, A.; Reza-San Germán, C. M.; Flores-Valle, S. O. Advances in the Transesterification of Triglycerides to Biodiesel Using MgO−NaOH, MgO−KOH and MgO−CeO₂ as Solid Basic Catalysts. *Catal. Today* **2013**, *212*, 23−30.

(62) Yoshikawa, K.; Kaneeda, M.; Nakamura, H. Development of Novel CeO2-Based CO2 Adsorbent and Analysis on Its CO₂ Adsorption and Desorption Mechanism. *Energy Procedia* **2017**, *114*, 2481−2487.

(63) Hu, J.; Zhu, K.; Chen, L.; Kübel, C.; Richards, R. MgO(111) Nanosheets with Unusual Surface Activity. *J. Phys. Chem. C* **2007**, *111*, 12038−12044.

(64) Xu, S.; Zeng, H.-Y.; Cheng, C.-R.; Duan, H.-Z.; Han, J.; Ding, P.-X.; Xiao, G.-F. Mg-Fe mixed oxides as solid base catalysts for the transesterification of microalgae oil. *RSC Adv.* **2015**, *5*, 71278−71286.

(65) Khatun, R.; Biswas, S.; Biswas, I. H.; Riyajuddin, S.; Haque, N.; Ghosh, K.; Islam, S. M. Cu-NPs@ COF: A Potential Heterogeneous Catalyst for CO₂ Fixation to Produce 2-Oxazolidinones as Well as Benzimidazoles under Moderate Reaction Conditions. *J. CO₂ Util.* **2020**, *40*, 101180.

(66) Phatake, V. V.; Bhanage, B. M. Cu@ UgC₃N₄ Catalyzed Cyclization of O-Phenylenediamines for the Synthesis of Benzimidazoles by Using CO₂ and Dimethylamine Borane as a Hydrogen Source. *Catal. Lett.* **2019**, *149*, 347−359.

(67) Iijima, T.; Yamaguchi, T. K₂CO₃-Catalyzed Direct Synthesis of Salicylic Acid from Phenol and Supercritical CO₂. *Appl. Catal., A* **2008**, *345*, 12−17.

(68) Kathalikkattil, A. C.; Tharun, J.; Roshan, R.; Soek, H.-G.; Park, D.-W. Efficient Route for Oxazolidinone Synthesis Using Heterogeneous Biopolymer Catalysts from Unactivated Alkyl Aziridine and CO₂ under Mild Conditions. *Appl. Catal., A* **2012**, *447−448*, 107−114.

(69) Farooq, M.; Ramli, A.; Naeem, A.; Saleem khan, M. Effect of Different Metal Oxides on the Catalytic Activity of γ-Al₂O₃−MgO Supported Bifunctional Heterogeneous Catalyst in Biodiesel Production from WCO. *RSC Adv.* **2016**, *6*, 872−881.

(70) Zhao, W.; Li, H.; Li, Y.; Long, J.; Xu, Y.; Yang, S. Low-Cost Acetate-Catalyzed Efficient Synthesis of Benzimidazoles Using Ambient CO₂ as a Carbon Source under Mild Conditions. *Sustainable Chem. Pharm.* **2020**, *17*, 100276.

(71) Shen, Q.; Chen, X.; Tan, Y.; Chen, J.; Chen, L.; Tan, S. Metal-Free N-Formylation of Amines with CO₂ and Hydrosilane by Nitrogen-Doped Graphene Nanosheets. *ACS Appl. Mater. Interfaces* **2019**, *11*, 38838−38848.

(72) Grover, J.; Roy, S. K.; Jachak, S. M. Potassium Carbonate-Mediated Efficient and Convenient Synthesis of 3-Methyl-1-

phenylchromeno[4,3-c]pyrazol-4(1H)-ones. *Synth. Commun.* **2014**, *44*, 1914−1923.

(73) Fang, C.; Lu, C.; Liu, M.; Zhu, Y.; Fu, Y.; Lin, B.-L. Selective Formylation and Methylation of Amines Using Carbon Dioxide and Hydrosilane Catalyzed by Alkali-Metal Carbonates. *ACS Catal.* **2016**, *6*, 7876−7881.

(74) Fujii, A.; Choi, J.-C.; Fujita, K. Quaternary Ammonium Salt-Catalyzed Carboxylative Cyclization of Propargylic Amines with CO_2. *Tetrahedron Lett.* **2017**, *58*, 4483−4486.

(75) Weerakkody, C.; Rathnayake, D.; He, J.; Dutta, B.; Kerns, P.; Achola, L.; Suib, S. L. Enhanced Catalytic Properties of Molybdenum Promoted Mesoporous Cobalt Oxide: Structure-Surface-Dependent Activity for Selective Synthesis of 2-Substituted Benzimidazoles. *ChemCatChem* **2019**, *11*, 528−537.

(76) Yu, B.; Zhang, H.; Zhao, Y.; Chen, S.; Xu, J.; Hao, L.; Liu, Z. DBU-Based Ionic-Liquid-Catalyzed Carbonylation of o-Phenylenedi-amines with CO_2 to 2-Benzimidazolones under Solvent-Free Conditions. *ACS Catal.* **2013**, *3*, 2076−2082.

⧉ Recommended by ACS

Nature-Inspired Photoactive Metal–Organic Framework Nanofiber Filters for Oil–Water Separation: Conserving Successive Flux, Rejection, and Antifouling

Karthikeyarajan Vinothkumar, R. Geetha Balakrishna, *et al.*

JANUARY 03, 2023
INDUSTRIAL & ENGINEERING CHEMISTRY RESEARCH   READ ☑

Electrochemical, Ultrasensitive, and Selective Detection of Nitrite and H_2O_2: Novel Macrostructured Phthalocyanine with Composite MWCNTs on a Modified GCE

, Bhari Mallanna Nagaraja, *et al.*

JANUARY 16, 2023
LANGMUIR   READ ☑

Highly Cross-Linked 3D ε-Fe_2O_3 Networks Organized by Ultrathin Nanosheets as High-Performance Anode Materials for Lithium-Ion Storage

Deli Li, Li Li, *et al.*

FEBRUARY 14, 2023
ACS APPLIED NANO MATERIALS   READ ☑

Synthesis, Molecular Docking, Dynamics, Quantum-Chemical Computation, and Antimicrobial Activity Studies of Some New Benzimidazole–Thiadiazole Hybrids

Ismail Celik, Zafer Asım Kaplancıklı, *et al.*

DECEMBER 09, 2022
ACS OMEGA   READ ☑

Get More Suggestions >